JOURNAL OF COMPUTATIONAL PHYSICS **134,** 31–61 (1997)
ARTICLE NO. CP975692

Unsplit Schemes for Hyperbolic Conservation Laws with Source Terms in One Space Dimension

Miltiadis V. Papalexandris, Anthony Leonard, and Paul E. Dimotakis

Graduate Aeronautical Laboratories, California Institute of Technology, Pasadena, California 91125
E-mail: milto@hydra0.caltech.edu

Received February 12, 1996; revised February 17, 1997

The present work is concerned with an application of the theory of characteristics to conservation laws with source terms in one space dimension, such as the Euler equations for reacting flows. Space-time paths are introduced on which the flow/chemistry equations decouple to a characteristic set of ODE's for the corresponding homogeneous laws, thus allowing the introduction of functions analogous to the Riemann invariants in classical theory. The geometry of these paths depends on the spatial gradients of the solution. This particular decomposition can be used in the design of efficient unsplit algorithms for the numerical integration of the equations. As a first step, these ideas are implemented for the case of a scalar conservation law with a nonlinear source term. The resulting algorithm belongs to the class of MUSCL-type, shock-capturing schemes. Its accuracy and robustness are checked through a series of tests. The stiffness of the source term is also studied. Then, the algorithm is generalized for a system of hyperbolic equations, namely the Euler equations for reacting flows. A numerical study of unstable detonations is performed.

1. INTRODUCTION

A variety of efficient numerical schemes for hyperbolic systems of conservation laws has been developed in the recent past. These schemes evolved following the understanding of fundamental concepts from the theory of nonlinear hyperbolic PDE's, such as characteristic surfaces, existence, uniqueness, and solution of the Riemann problem, etc. See, for example, Courant and Hilbert [11], Lax [27, 28], and Yee [56] for a review of the literature. The main application of these schemes was compressible, nonreacting flow.

Higher-order schemes, such as the ENO schemes (Harten *et al.* [21]), the MUSCL scheme (van Leer [53]), the PPM scheme (Colella and Woodward [10]), and Roe's approximate Riemann solver [45], can be viewed as extensions of Godunov's original scheme to second-order accuracy. This is done by making use of the theory of characteristics for systems of hyperbolic PDE's in one space dimension. They employ the characteristic decomposition of the equations into a set of scalar fields, locally (at each computational cell), to evaluate the flux terms at the cell interfaces. Discontuous solutions can be computed by supplementing the characteristic equations with appropriate jump relations, i.e., by solving the corresponding local Riemann problem.

Research in detonating flows was pioneered by Von Neumann [55], Zeldovich [57], and Doering [14] 50 years ago and, subsequently, by others. Numerical integration of the governing equations, in high-resolution meshes, was initiated by Fickett and Wood [18]. In the past, progress was achieved in the study of the stability (see, e.g., Erpenbeck [16], Lee and Stuart [29]) and the high- and low-frequency asymptotic nature of detonations (see, e.g., DiPerna and Majda [13], Majda and Rosales [36, 37], Choi and Majda [8], Majda and Roytburd [38], Kapila *et al.* [23]).

Accurate algorithms for gas dynamics were first employed in detonation problems in the late 1980s, using splitting techniques (see, e.g., Colella *et al.* [9], and Yee [56]). Further development of these codes and extensive numerical investigations were carried through to the 1990s (see, e.g., Bourlioux *et al.* [5], Lappas *et al.* [25], Pember [43], Quirk [44], LeVeque and Shyue [31]). These algorithms employed a splitting technique, i.e., integration of the gasdynamic terms of the equations first, and integration of the appropriate ODE for the source term in an intermediate step.

This decoupling can be done in an optimal way using Strang-type [50] splitting. Bounds for the $\mathscr{L}_1$ errors of splitting methods have been established for scalar conservation laws by Crandall and Majda [12] for dimensional splitting in multidimensional homogeneous equations and by Tang and Teng [51] for time-splitting in 1D scalar laws with source terms. Nevertheless, this decoupling introduces numerical errors. The decomposition of the equations into scalar fields is not straightforward; i.e., the quantities known as Riemann invariants are now not constant along the characteristic trajectories. Such an error can be significant in systems with multimode instabilities and multiplicity of spatial and temporal scales, such as the Euler equations for reacting flows.

So far, efforts to design unsplit schemes had been based on the idea of modifying the Riemann problem on the cell

0021-9991/97 $25.00

interfaces, to take care of the presence of the source terms. This idea of a generalized Riemann problem was introduced by Liu [34] for quasi-one-dimensional (area-varying) gas flows. He considered a Riemann problem, where the initial data were not uniform on each cell but satisfied the steady-state equations, to construct a random-choice method to prove the existence of global solutions for the nonhomogeneous system of equations. Glimm *et al.* [19], and van Leer [54] derived second-order accurate schemes for such flows based on this idea. Roe [46, 47] proposed the addition of extra terms in the expressions of the wave strengths in Roe's approximate Riemann solver [45] that take the source terms into account. Ben-Artzi and Falcovitz [3], also concerned with area-varying flows, considered a Riemann problem for the nonhomogeneous equations with linearly distributed initial states. They derived expressions for the time derivatives of the unknown variables and their fluxes by solving this Riemann problem and then used these expressions in the upwinding step of their algorithm. Application of this strategy to unsplit schemes for reacting flows was presented by Ben-Artzi [2].

An alternate approach was recently introduced by Lappas *et al.* [26] who developed an unsplit MUSCL-type scheme for the 2D compressible equations. The equations of motion of a compressible, nonreacting fluid, along the characteristics in two and three space dimensions, are not homogeneous. They include a kinematic, source-like term that is proportional to the in-plane divergence of the velocity field, i.e., the two-component divergence in the plane locally perpendicular to the classical characteristic (Lappas *et al.* [26, Eq. (46) and related discussion]). As a consequence, the classical characteristics do not serve as paths for Riemann invariants in more than one space dimension. In the analysis by Lappas *et al.* [26], a general methodology is developed that defines manifolds in space-time, dubbed as "Riemann invariant manifolds," along which the equations are decomposed into the same scalar fields as in the 1D case and solved numerically. These manifolds may appear to be space-like, or time-like, in the classical description, depending on the flow-velocity gradients, but they embed the paths along which the characteristic equations apply (exactly).

In the present paper, the work of Lappas *et al.* [26] is extended to systems of hyperbolic conservation laws with source terms, such as compressible, reacting flows. For one-dimensional systems, a set of paths is defined in space-time, such that the equations that hold along these paths are the same as the equations that hold along the characteristics in the corresponding homogeneous case. As in the case discussed by Lappas *et al.*, the local geometry of these paths depends on the spatial derivatives of the flow variables, as well as on the source terms themselves. These paths facilitate the design of unsplit algorithms. In particular, an effort was made to improve the performance of the MUSCL-type schemes by constructing algorithms in which the integration of the equations, including the contributions of the source terms, is performed in a single, fully coupled step. This is achieved by tracing the corresponding invariant paths, in a way analogous to characteristic-tracing in the homogeneous case.

The first part of this paper deals with the development of these ideas for a scalar conservation law with a nonlinear source term. Extensive numerical experimentation has been conducted. The results are compared with approximate solutions, or exact solutions whenever possible. The role of the stiffness of the source term has also been examined. The second part deals with the unsteady, compressible, Euler equations for reacting flows in one space dimension. Comparisons with results obtained by conventional schemes are made.

2. THE INVISCID BURGERS EQUATION WITH A NONLINEAR SOURCE TERM

2.1. *General Formulation*

Consider the following initial value problem for the scalar $u(x, t)$:

$$\frac{\partial}{\partial t} u + \frac{\partial}{\partial x} f(u) = g(u), \quad x \in [0, \infty), \tag{2.1a}$$

$$u(x, 0) = u_0(x) \in [0, 1]. \tag{2.1b}$$

The corresponding homogeneous law is associated with a convex entropy pair, i.e., the entropy function: $\phi(u)$, and the entropy flux: $\psi(u)$, satisfying

$$\psi_u = \phi_u f_u.$$

The entropy pair is subject to the following entropy condition:

$$\frac{\partial}{\partial t} \phi(u) + \frac{\partial}{\partial x} \psi(u) \leq 0. \tag{2.2}$$

Furthermore, the source term, $g(u)$, is assumed to satisfy

$$g(u) \in \mathscr{C}^2([0, 1], \mathscr{R}), \tag{2.3a}$$

$$g(0) = 0 = g(1). \tag{2.3b}$$

Let $\Omega = [0, \infty) \times [0, T]$. A bounded measurable function, u, is a weak solution of (2.1), if $\forall \xi \in \mathscr{C}^1(\Omega)$ with compact support in $([0, \infty) \times [0, T))$,

$$\int\int_\Omega (u\xi_t + f(u)\,\xi_x)\,\mathrm{d}x\,\mathrm{d}t + \int_0^\infty u_0(x)\,\xi(x, 0)\,\mathrm{d}x = -\int\int_\Omega \xi g\,\mathrm{d}x\,\mathrm{d}t. \tag{2.4}$$

Existence and uniqueness of weak solutions for this problem was given by Kruzkov [24]. The source term, $g(u)$, is constructed to possess two equilibrium values, at $u = 1$ and $u = 1$. The large-time solution of the above initial value problem may approach one equilibrium value, or another, depending on the nature of the source term. The decay estimates for the corresponding homogeneous law (Lax [27, 28]) do not hold for the above problem.

The characteristic decomposition of the problem yields:

$$\frac{\mathrm{d}u}{\mathrm{d}t} = g(u), \quad \text{along } \frac{\mathrm{d}x}{\mathrm{d}t} = f_u. \tag{2.5}$$

Motivated by the fact that for the corresponding homogeneous law, u remains constant along characteristics, someone could ask the question: Along which curve in space-time does u remain constant? The answer is that, at smooth parts of the flow,

$$\frac{\mathrm{d}u}{\mathrm{d}t} = 0, \quad \text{along } \frac{\mathrm{d}x}{\mathrm{d}t} = f_u - \frac{g(u)}{\partial u/\partial x}. \tag{2.6}$$

The geometry of this curve depends locally on the spatial derivatives of the solution. This, however, should not be disturbing because the derivatives are known for any time the solution itself is known, i.e., all the necessary elements to construct this curve in space-time are available, without extra cost.

2.2. *Description of the Algorithm and Numerical Results*

Consider the initial value problem formulated as above, when $f(u) = u^2/2$:

$$\frac{\partial}{\partial t}u + \frac{\partial}{\partial x}\left(\frac{u^2}{2}\right) = g(u), \quad x \in [0, \infty). \tag{2.7a}$$

$$u(x, 0) = u_0(x) \in [0, 1]. \tag{2.7b}$$

A typical nonlinear term satisfying (2.3a) and (2.3b) is

$$g(u) = \frac{1}{\varepsilon}u(1 - u), \tag{2.8}$$

where ε is a coefficient measuring the stiffness of the system. An entropy pair associated with the corresponding homogeneous law is given by

$$\phi(u) = u^2, \quad \psi(u) = \frac{2}{3}u^3. \tag{2.9}$$

In the case where the source term is given by (2.8), and for smooth $u_0(x)$, the equation of the characteristic decomposition yields

$$u(x, t) = u_0 \frac{e^{t/\varepsilon}}{1 + (e^{t/\varepsilon} - 1)u_0}, \tag{2.10a}$$

along the curves,

$$x = x_0 + \varepsilon \log[1 + (e^{t/\varepsilon} - 1)u_0]. \tag{2.10b}$$

Given the above relation, one can deduce the following shock-formation criterion: For the initial value problem given by (2.7) and (2.8), a shock is formed if the following inequality is satisfied:

$$u_0(x) + \varepsilon u_0'(x) < 0 \quad \text{for some } x, \tag{2.11}$$

where $u_0'(x)$ is the derivative of $u_0(x)$. The shock-formation time is given by

$$t_{\text{s.f.}} = \varepsilon \log\left(\frac{A(x) - 1}{A(x)}\right), \quad A(x) \equiv (u_0(x) + \varepsilon u_0'(x))_{\min}. \tag{2.12}$$

The equation of the constant-u curves is given by

$$\frac{\mathrm{d}x}{\mathrm{d}t} = u - \frac{g(u)}{\partial u/\partial x} \equiv v(x, t). \tag{2.13}$$

The issue of the limit case $\partial u/\partial x \to 0$ will now be addressed. First, it should be noticed that the equation is not singular at the points of the (x, t)-plane, where the spatial derivative of the solution becomes zero. The path defined by (2.13) becomes locally parallel to the x axis at those points. At such points, it cannot be used for the evaluation of the fluxes at the interfaces. Additionally, a nonzero, but very small, value of u_x (it can occur, say, in the cells neighboring the one, where $u_x = 0$) might lead to a large value of $v(x, t)$. Then, a small time-step would be necessary when (2.13) is to be integrated numerically, to maintain the desired-level of accuracy. For these isolated cases, it would be better to find the fluxes at the interfaces by employing a Taylor expansion. In the following, it is shown how these ideas can be combined in a simple and uniform manner.

A similar phenomenon can occur in the application of shock-capturing schemes for the numerical solution of Hamilton–Jacobi-type equations. A well-known example is the computation of moving fronts whose speed is curvature-dependent (Osher and Sethian [41], Sethian [48]). The equivalent situation there arises when the speed of the front is locally zero. No serious difficulties were reported in the computations at these points.

The algorithm proposed for the numerical integration of the above problem belongs to the class of second-order accurate MUSCL-type schemes and is described below.

Consider uniform spacing in the x direction, of length Δx, and let u_j^n be the average of u in the jth cell at time $t = n\Delta t$, i.e.,

$$u_j^n = \frac{1}{\Delta x}\int_{(j-1/2)\Delta x}^{(j+1/2)\Delta x} u(x, n\,\Delta t)\,\mathrm{d}x. \tag{2.14}$$

Assume linear interpolation of $u(x, n\Delta t)$ on each cell:

$$u(x, n\Delta t) = u_j^n + (u_x)_j x, \quad x \in \left[-\frac{\Delta x}{2}, \frac{\Delta x}{2}\right]. \tag{2.15}$$

The slope of $u(x, t)$ on each cell, $(u_x)_j$, can be computed using a standard TVD limiter. In the present algorithm, van Albada's limiter was chosen (van Leer [54]):

$$(u_x)_j = \mathrm{ave}(u_x^-, u_x^+), \tag{2.16a}$$

where,

$$u_x^- = \frac{u_j^n - u_{j-1}^n}{\Delta x}, \quad u_x^+ = \frac{u_{j+1}^n - u_j^n}{\Delta x}, \tag{2.16b}$$

$$\mathrm{ave}(a, b) \equiv \frac{a+b}{2}\left(1 - \frac{(a-b)^2}{a^2 + b^2 + c^2}\right), \tag{2.16c}$$

and c is a small number ($c^2 \ll 1$).

The conservation law (2.7) is approximated by the following explicit finite-difference scheme:

$$u_j^{n+1} = u_j^n - \frac{\Delta t}{\Delta x}\left(\frac{(u_{j+1/2}^{n+1/2})^2}{2} - \frac{(u_{j-1/2}^{n+1/2})^2}{2}\right) + \frac{\Delta t}{2}\left(g(u_{j+1/2}^{n+1/2}) + g(u_{j-1/2}^{n+1/2})\right). \tag{2.17}$$

In this relation, $u_{j+1/2}^{n+1/2}$ denotes the value of u at the right interface of the jth cell at a time $t = (n + 1/2)\,\Delta t$. It is evaluated by tracing the constant-u curve forward in time, as given by (2.13). This is done by locating the point, x_p, that lies on that curve and satisfies $u(x_p, n\Delta t) = u_{j+1/2}^{n+1/2}$:

$$\frac{\Delta x}{2} - x_p = \frac{\Delta t}{2}u(x_p, n\Delta t) - g(u(x_p, n\Delta t))\int_{n\Delta t}^{(n+1/2)\Delta t}\frac{\mathrm{d}t}{u_x}. \tag{2.18}$$

Assuming linear interpolation of both $u(x, t)$ and $g(u)$ at each cell, this relation gives

$$\frac{\Delta x}{2} - x_p = \frac{\Delta t}{2}(u_j^n + (u_x)_j x_p) - (g(u_j^n) + g_u(u_j^n)(u_x)_j x_p)\int_{n\Delta t}^{(n+1/2)\Delta t}\frac{\mathrm{d}t}{u_x}. \tag{2.19}$$

The integral appearing on the right-land side of (2.19) can be evaluated by the forward Euler method. Numerical experiments, however, showed that the accuracy of the algorithm can be improved by using trapezoidal rule with the right endpoint approximated by a Taylor series, i.e.,

$$\int_{n\Delta t}^{(n+1/2)\Delta t}\frac{\mathrm{d}t}{u_x} = \frac{\Delta t}{2}h(u_j^n, (u_x)_j),$$

where

$$h(u_j^n, (u_x)_j) \equiv \frac{1}{2}\left(\frac{1}{(u_x)_j} + \frac{1}{(u_x)_j + \dfrac{\Delta t}{2}(u_{xt})_j)}\right) \equiv \frac{\omega(u_j^n, (u_x)_j)}{(u_x)_j} \tag{2.20}$$

and

$$(u_{xt})_j = (u_x)_j\,(g_u(u_j^n) - (u_x)_j). \tag{2.21}$$

Equation (2.19) must be supplemented with the appropriate jump relations that take care of discontinuities, i.e., an appropriate Riemann problem has to be solved locally at the interface. The Riemann problem for the corresponding homogeneous law, i.e., the inviscid Burgers equation, admits a self-similar solution, depending on x/t only (see, for example, Lax [27]). For the nonhomogeneous conservation law, the Rankine–Hugoniot relation remains the same, but the rarefaction wave no longer admits a self-similar representation. However, as $x \to 0$ and $t \to 0$, the solution of the nonhomogeneous case approaches the self-similar solution of the corresponding homogeneous problem. Also note that, for locally smooth solutions, the process of solving the discretized version of the ODE that holds along the curve (2.13) is sufficient because it gives second-order accurate results. The solution of the Riemann problem has to be employed only if discontinuities are present. These discontinuities, however, are due to the convective terms of the conservation laws and not the source terms; hence the inclusion of the source terms gives just a higher order correction (for a detailed discussion on this subject, see Pember [43]). Therefore, the self-similar solution can be used for computational purposes without loss of accuracy. For the conservation law under consideration and given the fact that $u(x, t) > 0$ (thus only shocks that propagate to the right are acceptable), the numerical

solution of the Riemann problem reduces to the following procedure:

Let u_L, u_R the solution at the left and right side of the jth interface:

$$u_L = u_j^n + \frac{\Delta x}{2}(u_x)_j,$$

$$u_R = u_{j+1}^n - \frac{\Delta x}{2}(u_x)_{j+1},$$

and let $\Delta u = u_R - u_L$. Let $u(x_p, n\Delta t)$ be the value evaluated by tracing the invariant curve (2.13) in time, as described above, and let $v(x_p, n\Delta t)$ be the tangent of (2.13) passing through $(x_p, n\Delta t)$. Then, $u_{j+1/2}^{n+1/2}$ is given by

$$u_{j+1/2}^{n+1/2} = \begin{cases} u(x_p, n\Delta t), & \text{if } v(x_p, n\Delta t) > 0, \\ u(x_p, n\Delta t) - \Delta u, & \text{if } v(x_p, n\Delta t) < 0. \end{cases} \tag{2.22}$$

As mentioned above, in the absence of discontinuities, this procedure gives

$$u_{j+1/2}^{n+1/2} = u(x_p, n\Delta t) = u_j^n + \frac{\Delta t}{2}\frac{\left(\frac{\Delta x}{\Delta t} - u_j^n\right)(u_x)_j + g(u_j^n)\omega(u_j^n, (u_x)_j)}{1 + \frac{\Delta t}{2}(u_x)_j - \frac{\Delta t}{2}g_u(u_j^n)\omega(u_j^n, (u_x)_j)}. \tag{2.23}$$

At the limit $u_x \to 0$, this relation has no singularity and can be used even for that limiting case. The following expression, based on Taylor-series expansion, could also be used:

$$u_{j+1/2}^{n+1/2} = u_j^n + \frac{\Delta x}{2}(u_x)_j + \frac{\Delta t}{2}(u_t)_j. \tag{2.24}$$

We compare the performance of the proposed scheme with the use of (2.24), globally, below (both expressions result in second-order accurate schemes). The fact that, for this particular scalar conservation law, Taylor-series expansions are not necessary to avoid division by zero, cannot be easily generalized.

Finally, it should be noted that any interpolation procedure can be implemented with the algorithm, because the interpolation step is in principle independent of the nature (split or unsplit) of the scheme. This step, however, plays an important role in the accuracy of any shock-capturing method. This is more so in the present case, because efficiency and robustness of the scheme depend greatly on the accuracy with which the ''invariant'' curve (2.13) is known and, hence, on the accuracy with which the spatial derivatives of the solution are approximated.

As a first of the scheme, the source term given by (2.8) was considered, with $\varepsilon = 1$. Initial and boundary conditions (IC's and BC's) are given by

$$u_0(x) = \begin{cases} x(1-x), & \text{if } x \le 1, \\ 0, & \text{if } x > 1, \end{cases} \tag{2.25}$$

and

$$u(0,t) = 0, \quad u(\infty, t) = 0 \quad \forall t. \tag{2.26}$$

The results obtained for this problem are given in Fig. 1. For this test case, $CFL = 0.6$. A shock is formed at time $t = 0.61803$. The value of u behind the shock increases because of the source term, until $u = 1$, which is a stable equilibrium value (the value $u = 0$ is an unstable one). From then on, the shock propagates with a speed $s = 0.5$. The evolution process is captured quite well by the present scheme.

As a second test, the initial conditions of the previous problem are changed to

$$u_0(x) = \begin{cases} 1, & \text{if } \Delta x < x \le 1, \\ 0, & \text{if } x > 1, \text{ or } 0 < x < \Delta x. \end{cases} \tag{2.27}$$

The results obtained for this problem are given in Fig. 2. For this test case, $CFL = 0.6$. The left discontinuity, initially at $x = 1$, becomes a rarefaction wave. The head of this expansion, which is an ''acoustic'' disturbance, moves with characteristic speed $u_{\text{ch}} = 1.0$, while the tail stays at the origin because the characteristic speed there is zero. The right discontinuity moves with a shock speed $s = 0.5$. As soon as the head of the expansion reaches the shock, the shock starts to decay. This decay, however, stops because the source term eventually restores the postshock value at the upper equilibrium level.

Consider now the following Riemann problem:

$$u_0(x) = \begin{cases} 0, & \text{if } 0 \le x, \\ 1, & \text{if } x > 0. \end{cases} \tag{2.28}$$

For this problem, we can use (2.10a), (2.10b) to get the expression of the resulting rarefaction in closed form:

$$u(x,t) = \begin{cases} \dfrac{e^{t/\varepsilon}(e^{x/\varepsilon} - 1)}{e^{x/\varepsilon}(e^{t/\varepsilon} - 1)}, & \text{if } x \le t, \\ 1, & \text{if } x > t. \end{cases} \tag{2.29}$$

The computed rarefaction, as shown in Fig. 2 (and for times that the postshock value is 1.0, so that u gets the

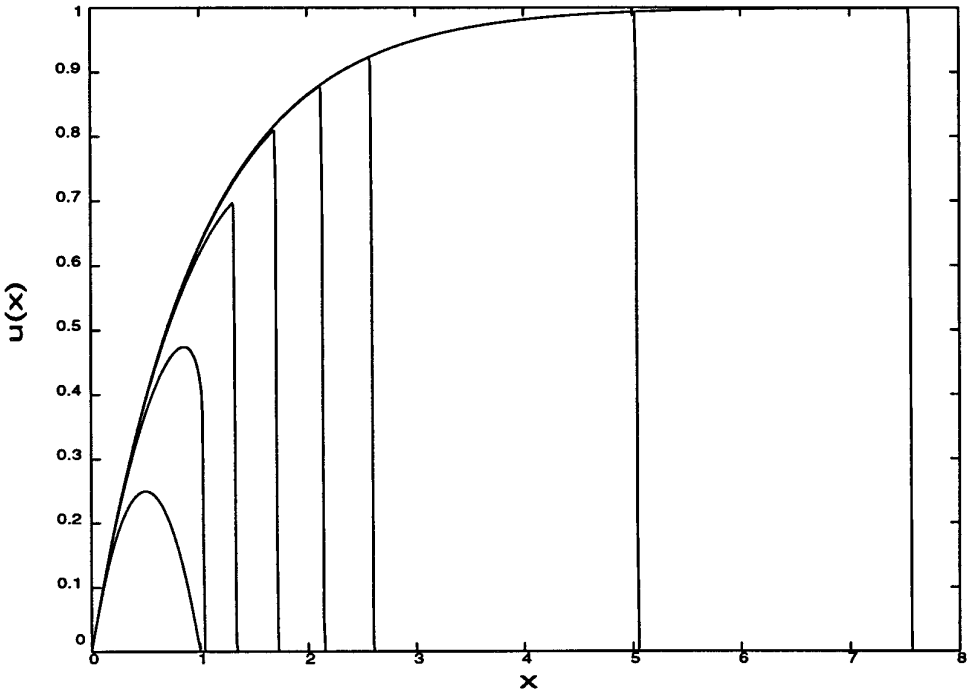

FIG. 1. Spatial profiles for the case where $g(u) = u(1 - u)$, and IC's, and BC's given by (2.25) and (2.26), respectively. Profiles at $t = 0.0, 1.0, 2.0, 3.0, 4.0, 5.0, 10.0, 15.0$. $\Delta x = 0.02$.

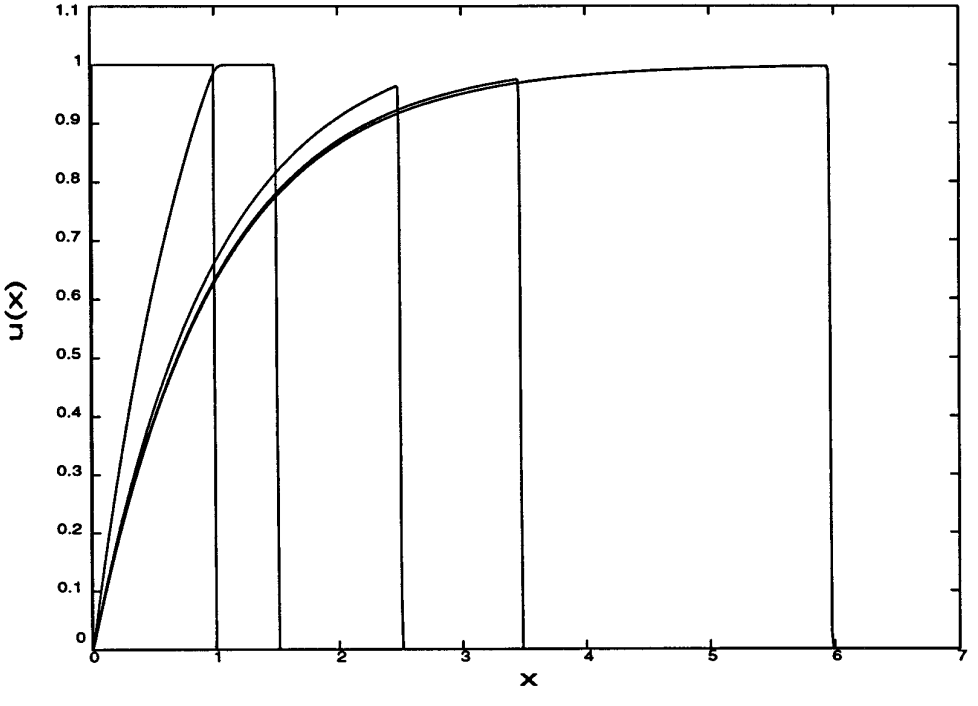

FIG. 2. Spatial profiles for the case where $g(u) = u(1 - u)$, and BC's, and IC's given by (2.26) and (2.27), respectively. Profiles at $t = 0.0, 1.0, 3.0, 5.0, 10.0$; $\Delta x = 0.02$.

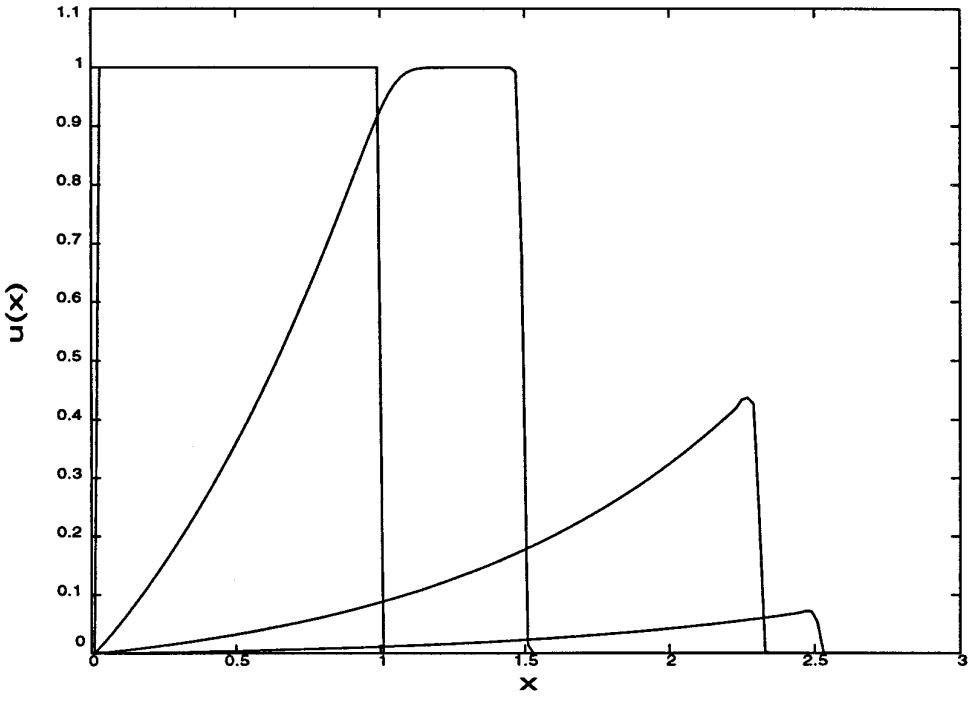

FIG. 3. Spatial profiles for the case where $g(u) = -u(1 - u)$, and BC's, and IC's given by (2.26) and (2.27), respectively. Profiles at $t = 0.0$, 1.0, 3.0, 5.0; $\Delta x = 0.02$.

equilibrium values at the endpoints of the rarefaction), are in excellent agreement with the above relation.

The same problem is also considered, but with a source term given by

$$g(u) = -u(1 - u). \tag{2.30}$$

The only difference with the previous problem is in the sign of the source term. The value $u = 1$ is now unstable while $u = 0$ is stable. Expressions for the characteristics and the shock-formation criterion can also be derived for this case. Numerical results for this problem are shown in Fig. 3. Again, they are obtained with $CFL = 0.6$. Note that the shock wave decays with a rate faster than $O(1/\sqrt{t})$, which is the decay rate for a shock wave in the corresponding homogeneous law.

The issue of the stiffness of the source term will now be discussed. Many authors have devoted attention to the numerical integration of hyperbolic PDEs with stiff source terms and the spurious solutions that might be obtained (e.g., Colella *et al.* [9], LeVeque and Yee [32], Bourlioux [4], Griffiths *et al.* [20], and Pember [42]). Even though shock-capturing schemes are stable, even in stiff cases, coarse spatial resolution may give incorrect propagation speeds of discontinuities. This is because the source terms are activated throughout the region occupied by the smeared shock, in a nonphysical manner. The result is a spurious shock speed, usually of one cell per time-step for coarse resolutions. It is also acknowledged (Bourlioux [4]) that finer temporal resolutions produces shock speeds of one cell per 2–3 time-steps. Pember [42] also pointed that out and additionally conjectured a criterion for the nonappearance of spurious solutions by implicit schemes for dissipative, 2×2 systems. The criterion was the commutability of the vanishing viscosity limit for viscous regularizations of (2.7) and the limit of infinite stiffness. Chen *et al.* [7] proved this commutability for such systems.

In the present numerical investigations, the focus is on the scalar law given by (2.7) and (2.8). The proposed scheme is compared with its equivalent split scheme, i.e.,

$$u^{n+1} = \mathscr{L}_{\mathrm{s}}^{(\Delta t/2)} \mathscr{L}_{\mathrm{f}}^{(\Delta t)} \mathscr{L}_{\mathrm{s}}^{(\Delta t/2)} (u^n). \tag{2.31}$$

Here, $\mathscr{L}_{\mathrm{f}}$ is the numerical solution operator for the corresponding homogeneous conservation law

$$\frac{\partial u}{\partial t} + \frac{\partial}{\partial x}\left(\frac{u^2}{2}\right) = 0. \tag{2.32a}$$

It is a MUSCL-type algorithm like the nonlinear version of Scheme III of van Leer [52]. The flux at the interfaces at time $t = (n + 1/2)\Delta t$ is evaluated by tracing the characteristic, $\mathrm{d}x/\mathrm{d}t = u$, and solving the Riemann problem associ-

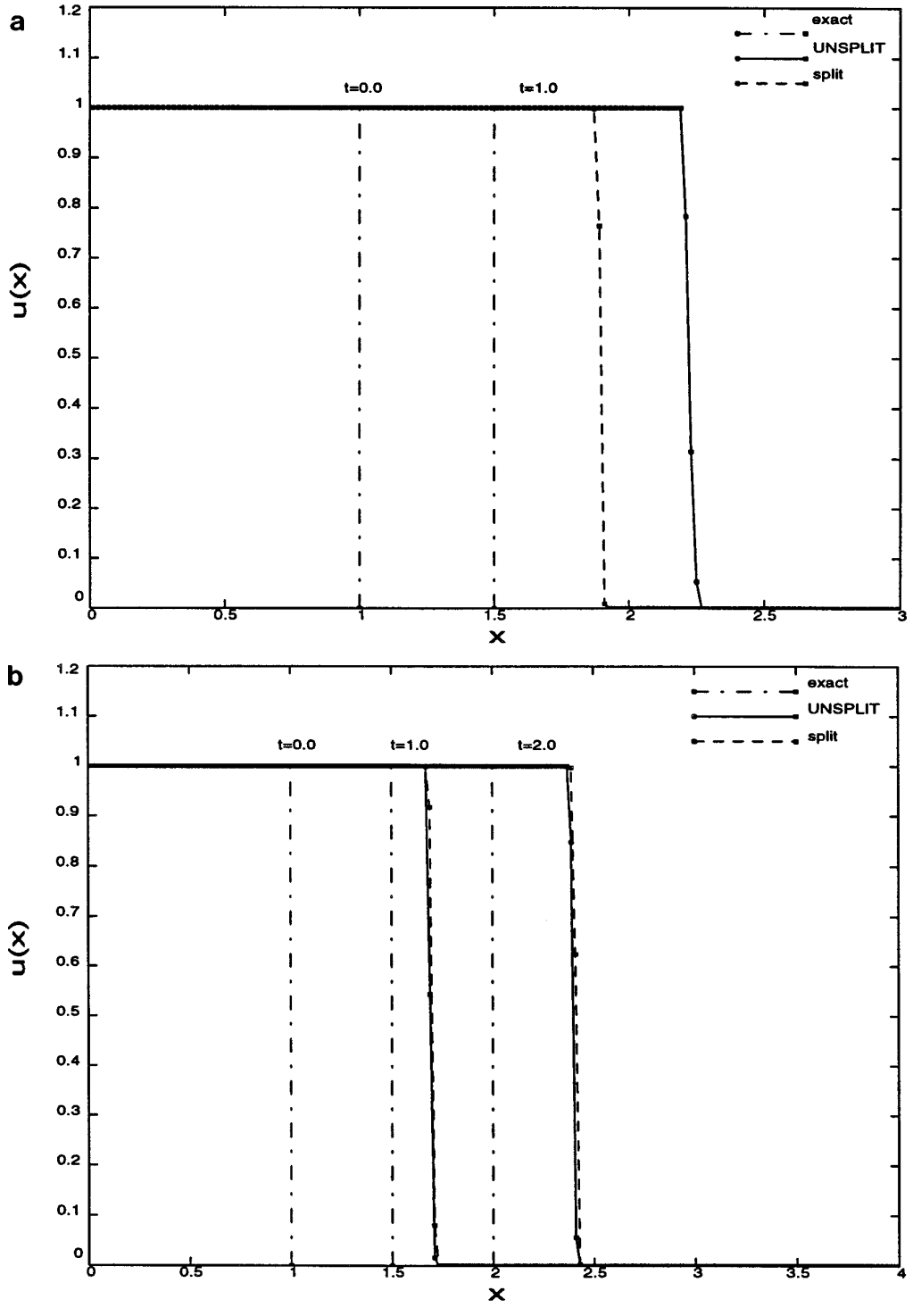

FIG. 4. Performance of unsplit and split algorithm for the problem given by (2.7), (2.8), (2.33), and (2.34), for $\varepsilon = 0.01$ (a); $\varepsilon = 0.02$ (b); $\varepsilon = 0.03$ (c); $\varepsilon = 0.05$ (d); $\varepsilon = 0.07$ (e).

ated with (2.32a). $\mathscr{L}_s$ is the numerical solution operator for the ODE,

$$\frac{du}{dt} = g, \tag{2.32b}$$

In the present work, $\mathscr{L}_s$ is chosen to be the second-order accurate, Runge–Kutta scheme. It could be argued that a more efficient split scheme could have been selected, such as an implicit one. But then again, the same is true for the unsplit scheme; the implicit version of the unsplit scheme

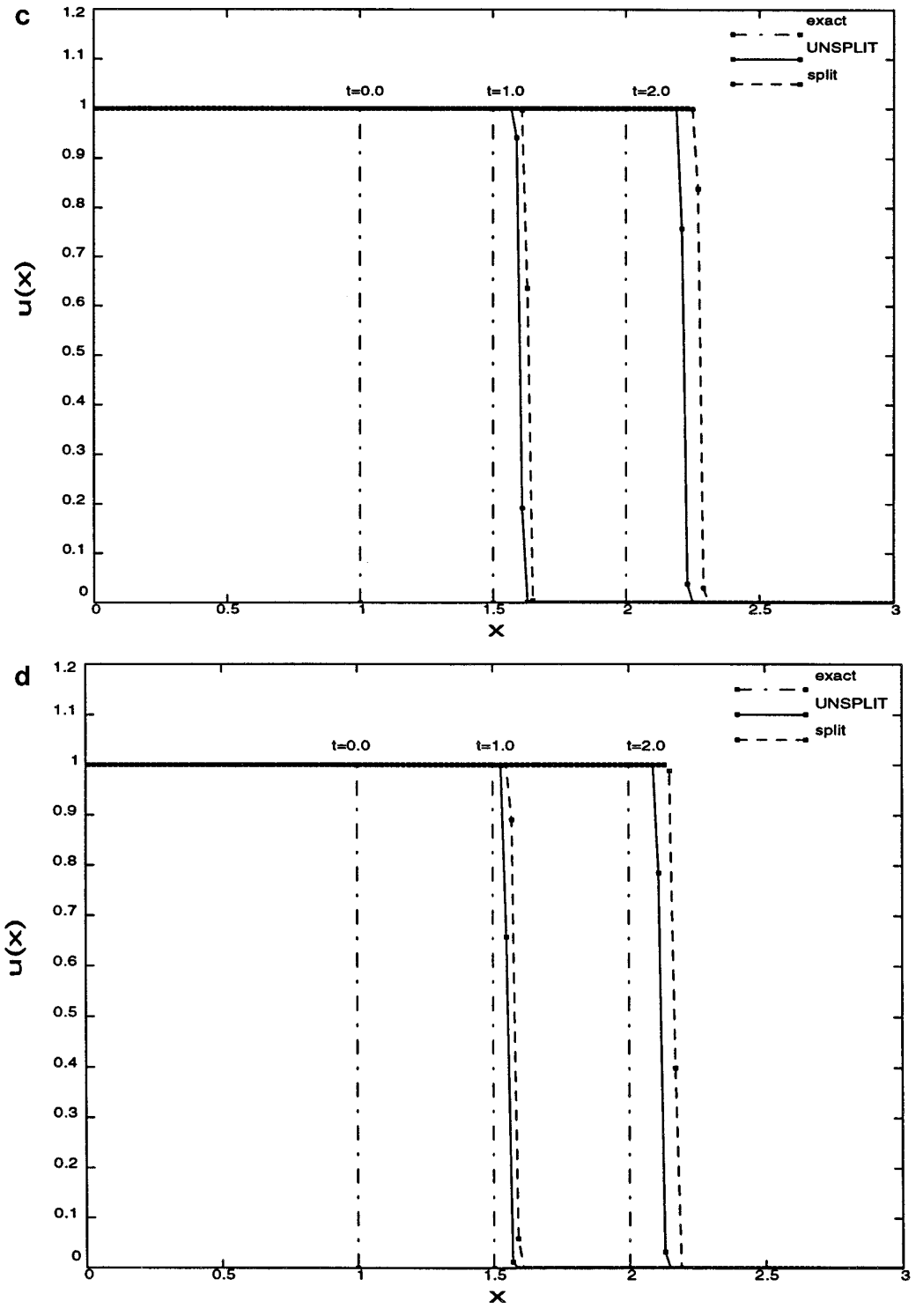

FIG. 4—*Continued*

for a scalar law can be easily implemented. The choice is made among second-order accurate schemes that had already been used in systems of PDEs such as the Euler equations. The MUSCL algorithm used in the split scheme is generally regarded as one of the most efficient algorithms.

For this study, the initial conditions were given by

$$u_0(x) = \begin{cases} 1, & \text{if } x \le 1, \\ 0, & \text{if } x > 1, \end{cases} \tag{2.33}$$

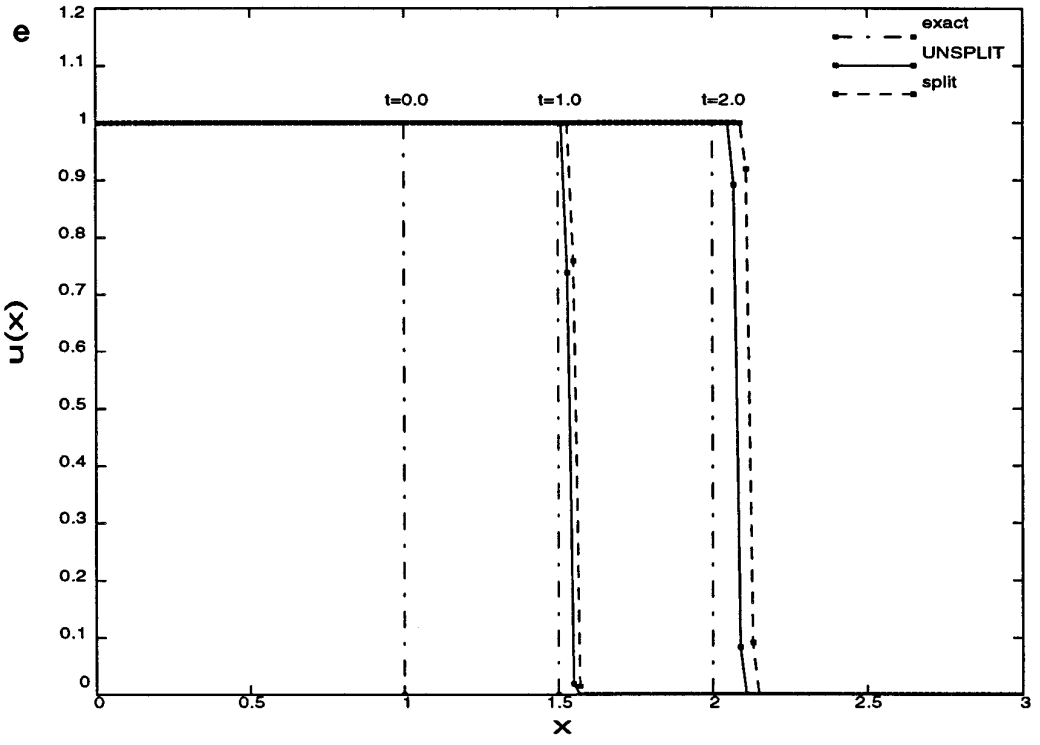

FIG. 4—*Continued*

with boundary conditions given by

$$u(0, t) = 1, \quad u(\infty, t) = 0 \quad \forall t. \tag{2.34}$$

For both algorithms, the discretization is $\Delta x = 0.02$ and the *CFL* number was 0.8. Results for $\varepsilon = 0.01$, 0.02, 0.03, 0.05, and 0.07 are given in Figs. 4.

Let s be the shock speed. For this problem $s = 0.5$. The relative error,

$$\frac{s_{\text{numerical}} - s_{\text{exact}}}{s_{\text{exact}}},$$

is plotted, for both schemes, in Fig. 5. The calculation of the numerical shock-wave speeds is based on the level set $u(x, t) = 0.5$. The split scheme gives a smaller error than the unsplit one in the regime $\Delta t/\varepsilon < 0.5$, but in that regime the relative error is above 40% for both schemes and would usually be unacceptable. The unsplit scheme seems to work slightly better than the split scheme, in the cases where the above ratio was small. For $\varepsilon > 0.1$, both schemes give an error less than 10%. For $\varepsilon < 0.01$, computed wave speeds are one cell per time step. The numerical solutions go unstable for $\varepsilon = O(10^5)$ with both schemes. Results for that test case are also obtained by the unsplit scheme (2.17) based on the Taylor-series expansion (2.24). The difference between the results given by that scheme and the ones given by the proposed (unsplit) scheme was negligible. Subsequently, the same test problem is solved with a smaller *CFL* number, namely *CFL* = 0.5. The changes in the numerical results are small for both schemes. This observation reflects the fact that both the spatial and the time discretization have to be small to avoid spurious solutions.

It is also interesting to mention that LeVeque and Yee [32] studied the equation

$$u_t + u_x = -\frac{1}{\varepsilon} u(u-1)\left(u - \frac{1}{2}\right),$$

with initial data given by (2.33). They used split algorithms to solve this problem and reported no spurious wave speeds for $\Delta t/\varepsilon \simeq 0.5$. This is most likely due to the difference in the source terms. For the source term in the above equation, the preshock value, $u = 0$, is a stable equilibrium. However, for the source term in the present work, the preshock value $u = 0$ is an unstable equilibrium. Consequently, values of $u(x, t)$ even slightly higher than 0 activate the source term which tends to increase u, until the stable equilibrium is attained.

Next, the issue of spurious continuous solutions is examined. As before, the conservation law (2.7) is considered

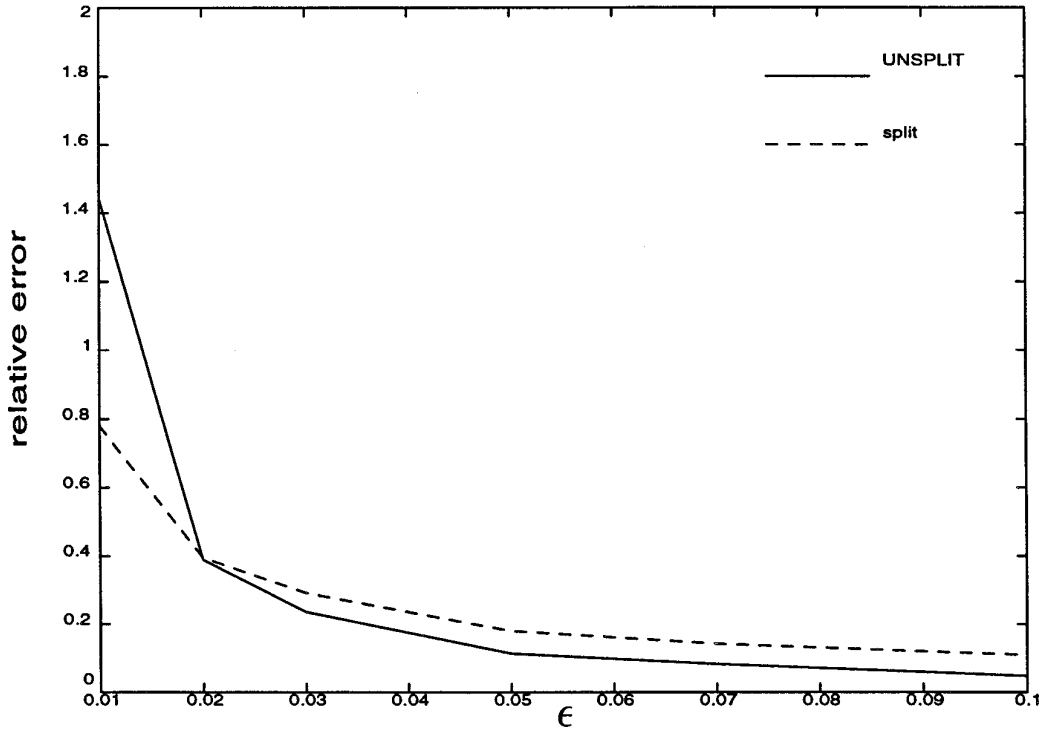

FIG. 5. Relative error for the split and unsplit algorithm for the problem given by (2.7), (2.8), (2.33), and (2.34).

with a source term given by (2.8). Initial and boundary conditions are given by

$$u_0(x) = e^{-x}, \tag{2.35}$$

$$u(0,t) = 1, \quad u(x \to \infty, t) = 0 \quad \forall t. \tag{2.36}$$

According to (2.11), a shock is never formed in this problem. Combining Eqs. (2.10a) and (2.10b), we deduce the following expression:

$$u(x,t) = \begin{cases} 1, & \text{if } x \le t, \\ e^{t-x}[u(x,t) + e^{t/\varepsilon}(1 - u(x,t))]^{1-\varepsilon}, & \text{if } x > t. \end{cases} \tag{2.37}$$

Then, for $\varepsilon \ll 1$, the following approximation holds:

$$u(x,t) = \begin{cases} 1, & \text{if } x \le t, \\ \dfrac{e^{-(x-t)}}{e^{-t/\varepsilon} + e^{-(x-t)}(1 - e^{-t/\varepsilon})}, & \text{if } x > t. \end{cases}$$

The acoustic disturbance at $x = t$, initially set at the origin, travels with a speed equal to unity. Then, for an extended region, the spatial decrease of $u(x,t)$ is very slow, i.e., $u(x,t)$ is *almost* equal to 1 within this region. The length of this region increases with time at a rate, $1/\varepsilon + 1$. After that region, the spatial decrease of $u(x,t)$ is exponential. Therefore, the solution to this problem is approximately an exponential profile, travelling with speed

$$c_{\text{e.p.}} = \frac{1}{\varepsilon} + 1.$$

Results for this case, obtained by the split scheme, the proposed unsplit scheme, and also by the unsplit scheme (2.17) based on the Taylor-series expansion (2.24), hereafter dubbed as "unsplit"—T.S.E.," are presented in Fig. 6 for $\varepsilon = 0.01$. The exact solution, computed from (2.37) using Newton iteration, is plotted for comparison purposes. It is seen that the proposed unsplit scheme and the MUSCL split scheme perform better than the unsplit scheme based on Taylor-series expansion. Furthermore, the proposed scheme is more accurate than the split one. The *CFL* number is taken at $CFL = 0.5$, for all schemes. When the *CFL* number is increased to 0.8, the proposed unsplit scheme is again more accurate than the split scheme (see Fig. 6c). For $\varepsilon = 0.01$, the relative error,

$$\left| \frac{c_{\text{numerical}} - c_{\text{e.p.}}}{c_{\text{e.p.}}} \right|,$$

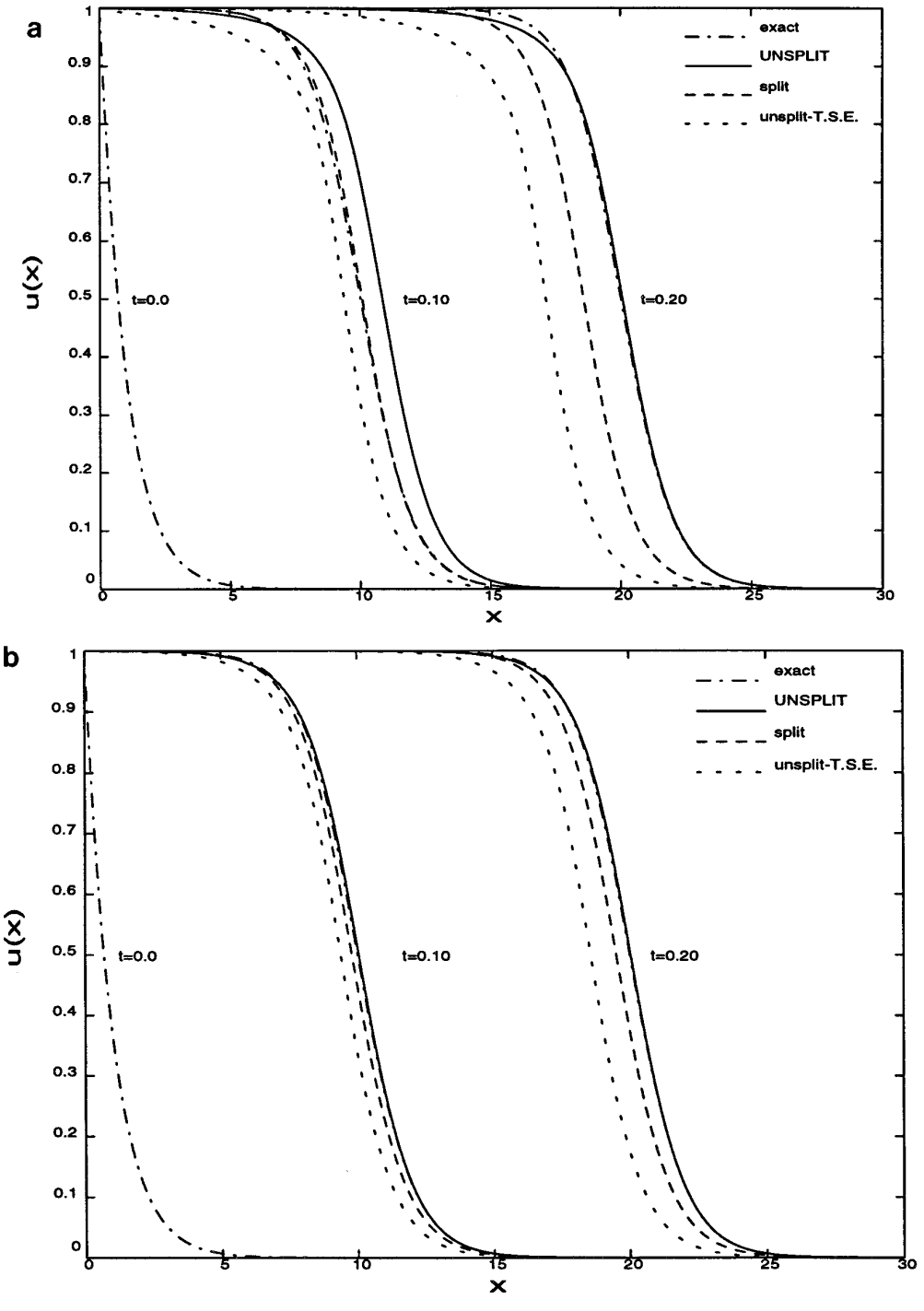

FIG. 6. Performance of unsplit and split algorithms for the problem given by (2.7), (2.8), (2.35), and (2.36) for $\varepsilon = 0.01$. $\Delta x = 0.03$, $CFL = 0.5$ (a); $\Delta x = 0.02$, $CFL = 0.5$ (b); $\Delta x = 0.02$, $CFL = 0.8$ (c).

in the calculation of the speed of the exponential front against the inverse of the resolution, $1/\Delta x$, is presented in Fig. 7, for all three schemes. The calculation of the numerical speed is based on the level set, $u(x, t) = 0.5$.

It is interesting to note that for this particular, shock-free case, an increase of Δx, with Δt held constant, does not seem to affect the accuracy of any of the schemes. It is found that fixing Δt, at a value of order $O(\varepsilon)$ and satisfying the CFL condition, is enough to produce reasonable results, even when Δx is an order of magnitude, or more,

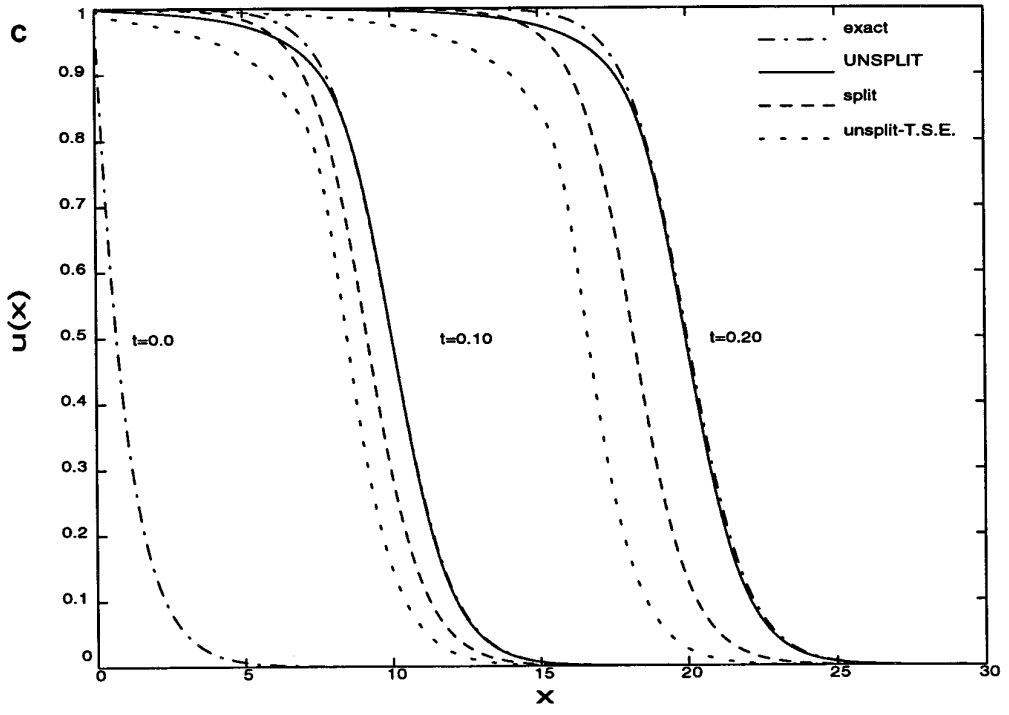

FIG. 6—*Continued*

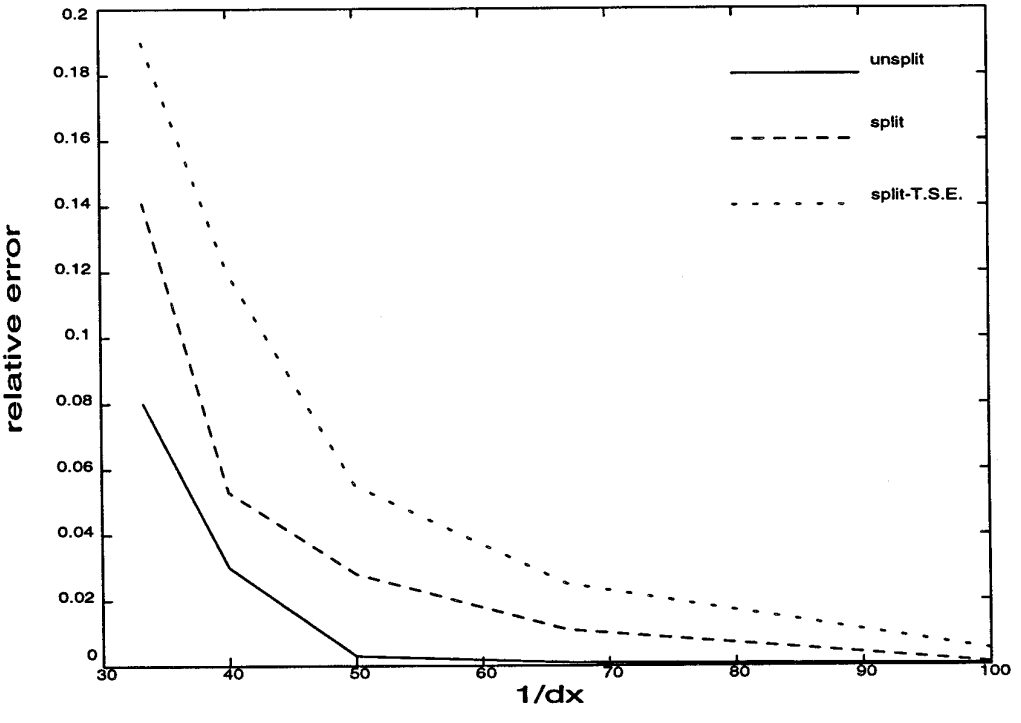

FIG. 7. Relative error in the calculation of the speed of the exponential front for the problem given by (2.7), (2.8), (2.35), and (2.36) for $\varepsilon = 0.01$. All computations were performed with $CFL = 0.5$.

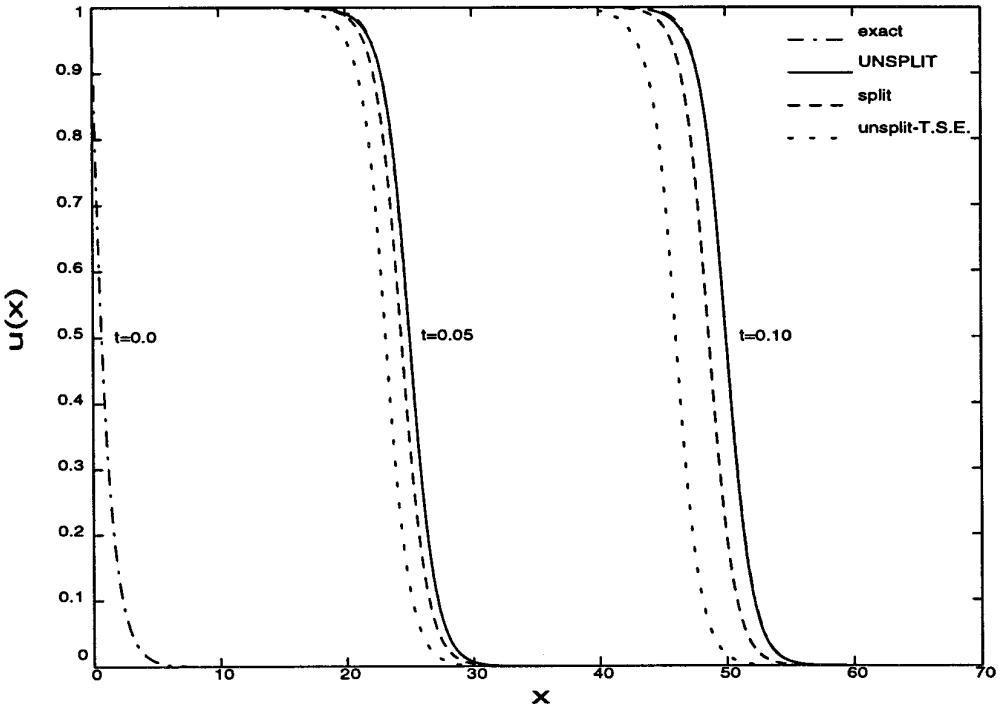

FIG. 8. Performance of unsplit and split algorithms for the problem given by (2.7), (2.8), (2.35), and (2.36) for $\varepsilon = 0.002$, $\Delta x = 0.004$, $CFL = 0.5$.

higher than $\Delta t|u|$. This observation is not valid in the case of discontinuous solutions, where both the spatial and the temporal discretization have to be of order $O(\varepsilon)$, or less, to avoid spurious shock waves.

The accuracy of the schemes remains at the same levels when the value of the stiffness coefficient is increased to $1/\varepsilon = 500$, with proportionally finer resolution. Again, the proposed unsplit scheme is slightly better than the split one, but both outperform the Taylor-series-based algorithm (see Fig. 8).

In summary, it was observed that neither the proposed scheme nor the split one give accurate wave speeds, if the time-step is not smaller than the stiffness coefficient, ε, when discontinuities are present. This is not surprising because both schemes are explicit and, therefore, good resolution of the smallest time scale is necessary. However, for reasonable time-steps, the proposed unsplit scheme is more accurate, particularly in cases characterized by a large value of the stiffness coefficient.

3. STUDY OF THE EULER EQUATIONS FOR CHEMICALLY-REACTING FLOWS

The decomposition for the scalar conservation law described above is extended to a system of equations in one space dimension. An unsplit numerical scheme has been designed based on this decomposition. The resulting scheme is used in the numerical study of unstable, one-dimensional detonations. The case of detonation problems is particularly interesting, as regards applications, but it is also difficult to simulate numerically. The difficulty arises from the large range of time scales and length scales associated with these problems.

3.1. *General Formulation*

A homogeneous, first-order system of n quasi-linear equations in two independent variables, (x, t),

$$\frac{\partial}{\partial t}\mathbf{U} + \frac{\partial}{\partial x}\mathbf{F}(\mathbf{U}) = 0, \tag{3.1}$$

is hyperbolic, if the Jacobian $\mathrm{D}\mathbf{F}(\mathbf{U})$ possesses real eigenvalues: $\lambda_i, i = 1, ..., n$. In the equation above, $\mathbf{U} = (u_1, ..., u_n)$ is the solution vector, and $\mathbf{F}(\mathbf{U})$ is the corresponding flux.

System (3.1) can be written in characteristic form:

$$\mathbf{l}_i \cdot \left(\frac{\mathrm{d}}{\mathrm{d}t}\mathbf{U}\right)_i = 0, \quad i = 1, ..., n \tag{3.2a}$$

(repeated index does not imply summation), with

$$\left(\frac{\mathrm{d}}{\mathrm{d}t}\right)_i \equiv \frac{\partial}{\partial t} + \lambda_i \frac{\partial}{\partial x}. \tag{3.2b}$$

This is done by performing the following steps:

1. Evaluate the eigenvalues of the Jacobian, $D\mathbf{F}(\mathbf{U})$, and the corresponding (left-) eigenvectors, i.e., $\mathbf{l}_i = (l_1, ..., l_n)_i$, $i = 1, ..., n$.

2. Take the scalar product of (3.1) with $\mathbf{l}_i$, $i = 1, ..., n$, produce the characteristic system (3.2).

There are important cases where the system (3.2) of ODEs is integrable. The equations describing isentropic, one-dimensional, gas-dynamic flows represent such an example. In such cases, the following relation holds:

$$\mathbf{l}_i \cdot \left(\frac{\mathrm{d}}{\mathrm{d}t}\mathbf{U}\right)_i = \left(\frac{\mathrm{d}}{\mathrm{d}t}R_i\right)_i = 0, \quad i = 1, ..., n. \tag{3.3}$$

The functions R_i, for $i = 1, ..., n$, are called Riemann invariants and are constant along the corresponding characteristic directions (cf. Eq. (3.2b)),

$$\frac{\mathrm{d}x}{\mathrm{d}t} = \lambda_i \quad \text{for } i = 1, ..., n. \tag{3.4}$$

In general, the system (3.2) is not integrable. Nevertheless, numerical evidence (coming mainly from results based on shock-capturing schemes for the one-dimensional Euler equations of gas dynamics, e.g., van Leer [53] and Colella and Woodward [10]) has shown that it it useful for numerical purposes to try to decompose the initial system of PDEs (3.1) to the characteristic set (3.2). The phrase *numerical purposes* can be interpreted as ''in order to develop algorithms that are both accurate and stable.'' In the homogeneous case, the system (3.2) holds along the characteristic lines (3.4).

The case of nonhomogeneous systems, i.e., for systems of the form

$$\frac{\partial}{\partial t}\mathbf{U} + \frac{\partial}{\partial x}\mathbf{F}(\mathbf{U}) = \mathbf{G}(\mathbf{U}), \tag{3.5}$$

the solution is not so straightforward. In this case, the set of Eqs. (3.2) does not hold along the characteristic paths (3.4). It is useful, however, to find the paths along which these equations hold. A straightforward calculation shows that the homogeneous ODEs (3.2) will hold along the new paths,

$$\frac{\mathrm{d}x}{\mathrm{d}t} = \lambda_i - \frac{\mathbf{l}_i \cdot \mathbf{G}(\mathbf{U})}{\mathbf{l}_i \cdot \partial\mathbf{U}/\partial x} \quad \text{for } i = 1, ..., n. \tag{3.6}$$

It is the system (3.2) that can be easily discretized and solved numerically, in the upwinding step of a shock-capturing solver. While this decomposition holds only at smooth parts of the flow, this is not a serious restriction. The numerical treatment of this decomposition is nonsmooth parts of the flow is completely analogous to the treatment of the characteristic decomposition when shocks are present, for the homogeneous case. Even though the characteristic decomposition in the homogeneous case holds only when the solution is continuous, it is still useful in the presence of shocks because it holds on either side of a discontinuity. Furthermore, the computation of these paths can be performed at no extra cost, since the information about the spatial derivatives of the flow is always available at points where the solution is known.

3.2. *Mathematical Formulation of the 1D Detonation Problem*

Consider a simple model of chemical interaction of two calorically perfect gases, $A \rightarrow B$, assuming one-step, irreversible, Arrhenius kinetics, and the absence of dissipation mechanisms. The conservation equations are given by

$$\frac{\partial}{\partial t}\rho + \frac{\partial}{\partial x}(\rho u) = 0, \tag{3.7a}$$

$$\frac{\partial}{\partial t}(\rho u) + \frac{\partial}{\partial x}(\rho u^2 + p) = 0, \tag{3.7b}$$

$$\frac{\partial}{\partial t}(\rho e_t) + \frac{\partial}{\partial x}[(\rho e_t + p)u] = 0, \tag{3.7c}$$

$$\frac{\partial}{\partial t}(\rho z) + \frac{\partial}{\partial x}(\rho u z) = \rho g(T, z). \tag{3.7d}$$

The total specific energy and the source term are given by

$$e_t \equiv \frac{p}{\rho(\gamma - 1)} + q_0 z + \frac{u^2}{2} \tag{3.8}$$

and

$$g(T, z) = -K z \exp(-E_a/T), \tag{3.9}$$

respectively, with the equation of state,

$$T = p/\rho. \tag{3.10}$$

In these equations, z is the reactant mass fraction, γ is the specific-heat ratio (assumed the same for both species), and q_0 is the heat-release parameter. E_a is the activation-energy parameter, and K is an amplitude parameter that sets the spatial and temporal scales. As employed here, $0 \leq z \leq 1$. It equals unity, when the material is totally unreacted, and zero when the reaction has been completed.

Despite the simplicity of this model, computing such flows is quite challenging. The reason is that for a wide range of values of the parameters of the reaction-rate equa-

tion, i.e., q_0, E_a, and K, this system of conservation laws is linearly and nonlinearly unstable. Furthermore, the reaction-rate equation is generally stiff and this leads to an extremely large range of (coupled) spatial and temporal modes. The resolution required for the numerical simulation of these flows typically exceeds available computational resources.

The system (3.7) can be written in conservation form, i.e., in the divergence form of (3.5) by setting

$$\mathbf{U} \equiv [u_1, u_2, u_3, u_4]^{\mathrm{T}} = [\rho, \rho u, \rho e_t, \rho z]^{\mathrm{T}}, \tag{3.11a}$$

$$\mathbf{F}(\mathbf{U}) \equiv \left[u_2, \frac{u_2^2}{u_1} + p, \frac{u_2}{u_1}(u_3 + p), \frac{u_2 u_4}{u_1} \right], \tag{3.11b}$$

$$\mathbf{G}(\mathbf{U}) \equiv [0, 0, -q_0(\gamma - 1)g, g]^{\mathrm{T}}, \tag{3.11c}$$

with

$$p = p(\mathbf{U}) = (\gamma - 1)\left(u_3 - \frac{u_2^2}{2u_1} - q_0 u_4 \right), \tag{3.12a}$$

$$g = g(\mathbf{U}) = -K u_4 \exp\left(-\frac{u_1 E_a}{p} \right). \tag{3.12b}$$

The eigenvalues of the system are

$$\lambda_1 = u + \sqrt{\gamma p/\rho}, \tag{3.13a}$$

$$\lambda_{2,3} = u, \tag{3.13b}$$

$$\lambda_4 = u - \sqrt{\gamma p/\rho}. \tag{3.13c}$$

The second/third eigenvalues are degenerate, therefore, z can sustain jumps only across contact discontinuities.

The following paths in the (x, t)-plane can be defined by performing the decomposition of the system to a set of ODEs, as described in the previous section,

$$\mathscr{C}_\pm : \frac{\mathrm{d}x}{\mathrm{d}t} = u \pm a + v_\pm, \tag{3.14a}$$

$$\mathscr{C}_0 : \frac{\mathrm{d}x}{\mathrm{d}t} = u + v_0, \tag{3.14b}$$

$$\mathscr{C}_r : \frac{\mathrm{d}x}{\mathrm{d}t} = u + v_r, \tag{3.14c}$$

with

$$a \equiv \sqrt{\gamma p/\rho},$$

the (frozen) speed of sound, and

$$v_\pm \equiv -\frac{K q_0(\gamma - 1)\rho z \exp(-E_a/T)}{\partial p/\partial x \pm \rho a(\partial u/\partial x)} \tag{3.15a}$$

$$v_0 \equiv -\frac{K q_0(\gamma - 1)\rho z \exp(-E_a/T)}{\partial p/\partial x - a^2(\partial \rho/\partial x)} \tag{3.15b}$$

$$v_r \equiv \frac{K z \exp(-E_a/T)}{\partial z/\partial x}. \tag{3.15c}$$

The ODEs along these paths are

$$\text{along } \mathscr{C}_\pm : \mathrm{d}p \pm \rho a \, \mathrm{d}u = 0, \tag{3.16a}$$

$$\text{along } \mathscr{C}_0 : \mathrm{d}p - a^2 \, \mathrm{d}\rho = 0, \tag{3.16b}$$

$$\text{along } \mathscr{C}_r : \mathrm{d}z = 0. \tag{3.16c}$$

There can be parts of the flow where the values of the added convection velocities, v_α, for $\alpha = 0, +, -, \mathrm{r}$, defined by (3.15) are small and the paths defined by (3.14) are very close to the corresponding (classical) characteristic paths. But there can also be parts of the flow where these are not negligible. In the latter case, the propagation speeds, $u \pm a + v_\pm$, will be considerably different from the classical characteristic speeds, $u \pm a$, and might even differ in sign. Interestingly, portions of these paths that emanate from some point, P, in the (x, t)-plane, might lie outside the region enclosed by the (classical) characteristics emanating from P, i.e., the domain of dependence of P. In such cases, the paths (3.14) might then be classified as locally space-like, otherwise locally time-like, in the classical description. These classifications, however, are based on the expressions for the characteristic speeds (3.4) of the system, $u \pm a$. Nevertheless, it is the (invariant) path equations given by (3.6) that are the ones along which the characteristic equations apply (exactly) and translate to the system (3.14) for the problem under study here.

3.3. *Description of the Numerical Scheme*

A second-order accurate MUSCL scheme, based on the above decomposition, is designed to solve the system of Eqs. (3.7) numerically. Consider a finite-volume formulation; i.e., space is discretized to a set of computational cells of length Δx. Additionally, consider mass-averaged values of the conservative variables

$$m_j \equiv \int_{x_{j-1/2}}^{x_{j+1/2}} \rho \, \mathrm{d}x, \tag{3.17a}$$

$$m_j u_j \equiv \int_{x_{j-1/2}}^{x_{j+1/2}} \rho u \, \mathrm{d}x, \tag{3.17b}$$

$$m_j m_{t\,j} \equiv \int_{x_{j-1/2}}^{x_{j+1/2}} \rho e_t \, \mathrm{d}x, \tag{3.17c}$$

$$m_j z_j \equiv \int_{x_{j-1/2}}^{x_{j+1/2}} \rho z \, \mathrm{d}x. \tag{3.17d}$$

Finally, set

$$m_j g_j \equiv \int_{x_{j-1/2}}^{x_{j+1/2}} \rho g(T, z)\, \mathrm{d}x. \tag{3.18}$$

In these expressions, average values of all quantities in the jth cell are denoted by the subscript j, while values of various quantities at the cell boundaries are denoted by $j + \frac{1}{2}$. By employing the following notation for the fluxes,

$$F_m \equiv \rho u, \tag{3.19a}$$

$$F_u \equiv \rho u^2 + p, \tag{3.19b}$$

$$F_e \equiv \rho e_{\mathrm{t}} u + p u, \tag{3.19c}$$

$$F_z \equiv \rho z u, \tag{3.19d}$$

the conservation equations at the jth cell are written as

$$\frac{\mathrm{d}}{\mathrm{d}t} m_j + (F_m)_{j+1/2} - (F_m)_{j-1/2} = 0, \tag{3.20a}$$

$$\frac{\mathrm{d}}{\mathrm{d}t} (m_j u_j) + (F_u)_{j+1/2} - (F_u)_{j-1/2} = 0, \tag{3.20b}$$

$$\frac{\mathrm{d}}{\mathrm{d}t} (m_j e_{\mathrm{t}\,j}) + (F_e)_{j+1/2} - (F_e)_{j-1/2} = 0, \tag{3.20c}$$

$$\frac{\mathrm{d}}{\mathrm{d}t} (m_j z_j) + (F_z)_{j+1/2} - (F_z)_{j-1/2} = m_j g_j. \tag{3.20d}$$

As in the case of the scalar conservation law, linear interpolation is used for all quantities on each cell. The slopes are estimated by van Albada's limiter (2.16). The proposed scheme, which evaluates the solution at time $(n + 1)\Delta t$ from the solution at the previous time $n\Delta t$, can be written as

$$(m_j)^{n+1} = (m_j)^n - \Delta t[(F_m)_{j+1/2}^{n+1/2} - (F_m)_{j-1/2}^{n+1/2}], \tag{3.21a}$$

$$(m_j u_j)^{n+1} = (m_j u_j)^n - \Delta t[(F_u)_{j+1/2}^{n+1/2} - (F_u)_{j-1/2}^{n+1/2}], \tag{3.21b}$$

$$(m_j e_{\mathrm{t}\,j})^{n+1} = (m_j e_{\mathrm{t}\,j})^n - \Delta t[(F_e)_{j+1/2}^{n+1/2} - (F_e)_{j-1/2}^{n+1/2}], \tag{3.21c}$$

$$(m_j z_j)^{n+1} = (m_j z_j)^n - \Delta t[(F_z)_{j+1/2}^{n+1/2} - (F_z)_{j-1/2}^{n+1/2} + (m_j g_j)^{n+1/2}]. \tag{3.21d}$$

The numerical fluxes $(F_m)_{j+1/2}^{n+1/2}$, $(F_u)_{j-1/2}^{n+1/2}$, $(F_e)_{j+1/2}^{n+1/2}$, $(F_z)_{j-1/2}^{n+1/2}$ are given by Eqs. (3.19). The quantities on the right-hand side of (3.19) are evaluated by solving the set of ODEs (3.16) numerically along the trajectories defined by (3.14). The case where a denominator in the expressions for v_+, v_-, v_0, v_{r} vanishes is treated in the same way as in the scalar law. Since the points of vanishing denominators are not points of singularity and only points of locally zero convection, the necessary information for upwinding can be obtained using a Taylor expansion in time. This procedure ensures, uniformly, second-order accuracy, in both space and time, for smooth parts of the flow.

The above set of ODEs must be supplemented with the appropriate jump relations to accommodate discontinuities, where a Riemann problem must be solved locally at each cell interface. The exact jump relations must generally be used in cells where the density and pressure slopes are large. The acoustic (isentropic) approximation can be used otherwise. A detailed description of the Riemann solver that was used can be found in Lappas *et al.* [25].

The Riemann problem that corresponds to this set of equations, referred as "generalized Riemann problem" (GRP), is not the same as the classical, one-dimensional, gasdynamic Riemann problem (RP). The GRP is not a self-similar problem and its solution is more complicated. The shock and expansion waves are curved in the (x, t)-plane, i.e., they are accelerating. The solution to the GRP has been worked out by Ben-Artzi [2], who showed that the solution approaches the solution of the RP in the limit $x \to 0$ and $t \to 0$. The use of the classical Riemann problem for numerical purposes is, therefore, justified by the same arguments that were mentioned earlier in this work, in the discussion of scalar laws. It is verified later that, using this approximation, the acceleration of the various waves can be captured numerically quite well.

3.4. *Numerical Results for 1D Detonations*

In the early 1940s, Zeldovich [57], von Neumann [55], and Doering [14], independently proposed that detonation waves in one-dimensional flows are steady shock waves, propagating in a medium of local thermodynamic equilibrium and followed by a reaction zone of finite length. This theory is historically known as the ZND theory of detonations. Given a fixed state ahead of the detonation, the computation of the spatial profiles of the solution reduces to the numerical integration of a nonlinear ODE; see Fickett and Davis [17]. Typical spatial ZND profiles for the pressure and the reactant mass fraction are given in Figs. 9.

For the detonations governed by the one-step irreversible Arrhenius law (3.9), there is a minimum shock velocity. This is the Chapman–Jouguet velocity, D_{CJ}. A reaction process characterized by this shock velocity is called a Chapman–Jouguet detonation. The point at the end of the reaction zone of a Chapman–Jouguet detonation is sonic. For every detonation, the shock velocity, D, has to satisfy $D \geq D_{\mathrm{CJ}}$. The parameter f, defined as

$$f \equiv \left(\frac{D}{D_{\mathrm{CJ}}}\right)^2,$$

is the overdrive factor of the detonation. The half-reaction length, $L_{1/2}$, i.e., the distance between the shock wave and

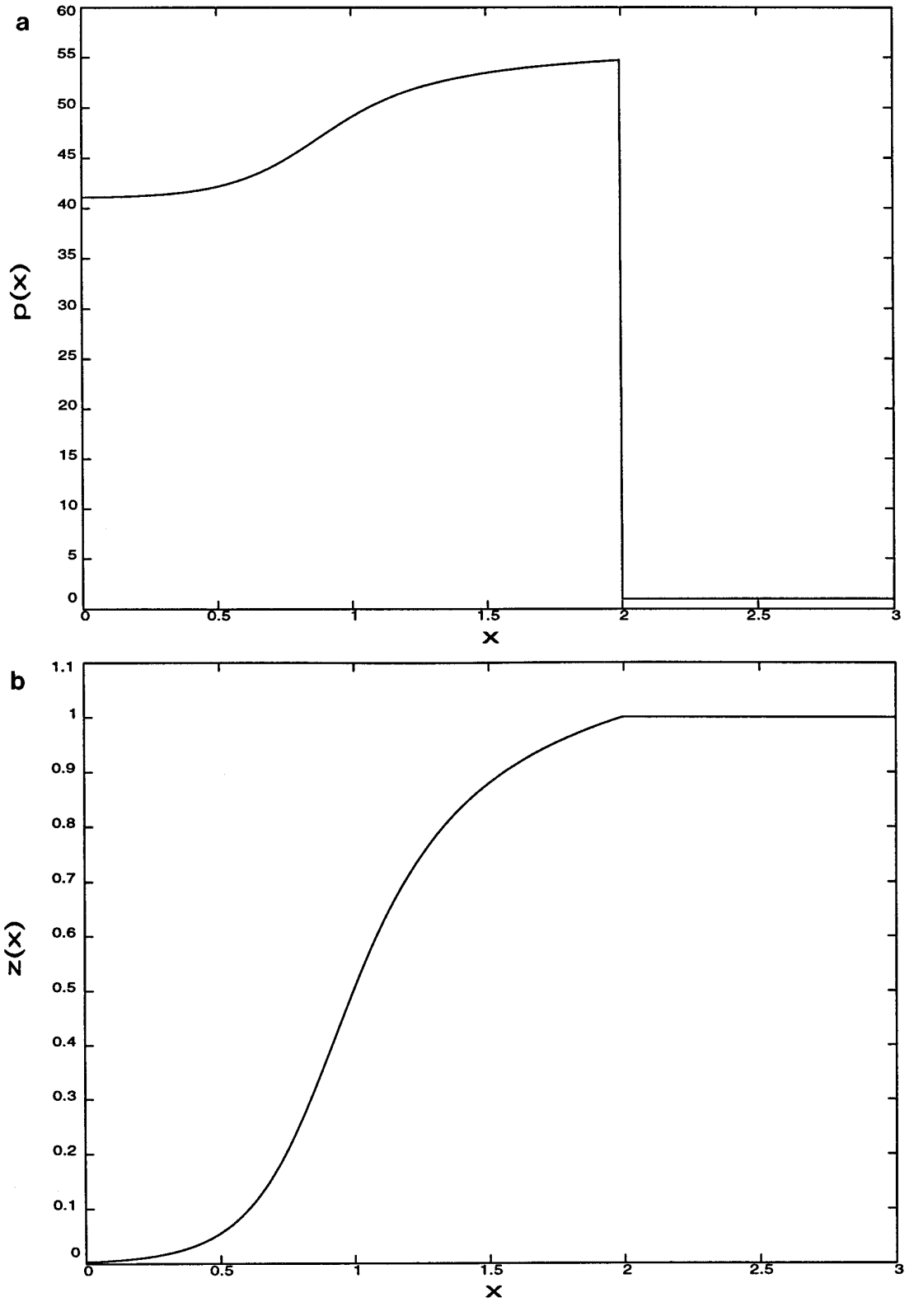

FIG. 9. (a) Typical spatial profile of the pressure for a ZND detonation. (b) Typical spatial profile of the reactant mass fraction for a ZND detonation.

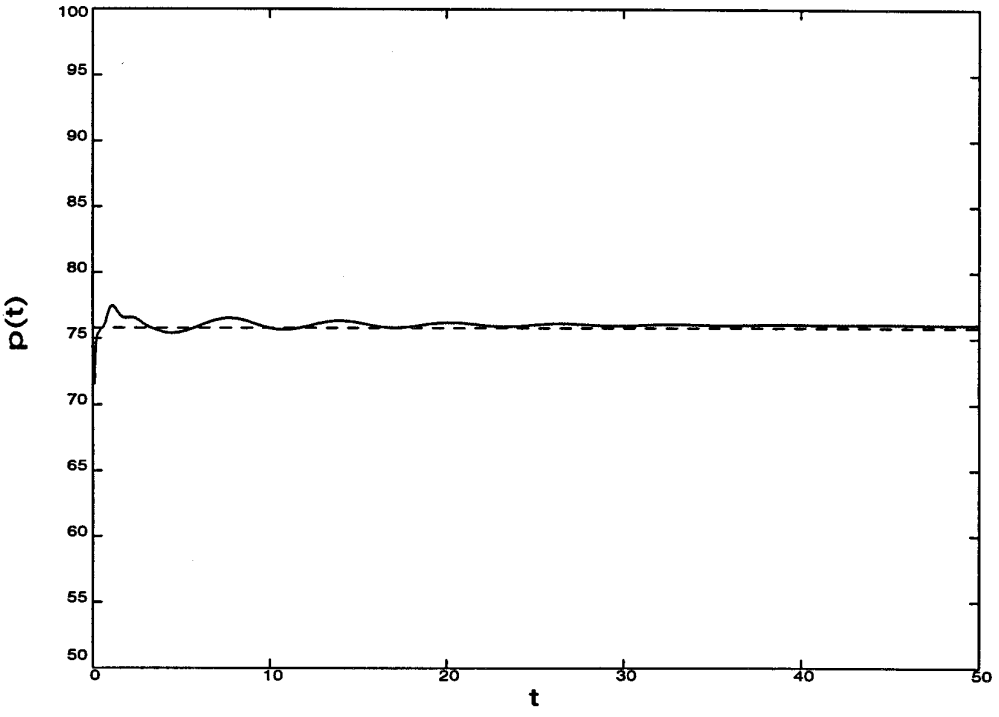

FIG. 10. Shock pressure time history for a detonation with an overdrive factor, $f = 1.80$. Resolution, 15 pts/$L_{1/2}$. Horizontal line represents ZND solution.

the point where $z = 0.5$, has been used as unit length throughout.

Experimental studies suggest, in contrast with the ZND theory, that detonation phenomena are generally unstable and possess a far more complicated structure (see, e.g., Fickett and Davis [17]). Linear-stability analysis of the conservation equations (3.7), by Erpenbeck [16] and Lee and Stewart [29] verify that the system is unstable for a large range of the parameters γ, q_0, E_a, and f.

In the following, the variables and the parameters of the system have been made dimensionless by reference to the uniform state ahead of the detonation front; hence f becomes the stability parameter of the system. The remaining parameters have been fixed as follows:

$$\gamma = 1.2, \quad q_0 = 50, \quad E_a = 50.$$

According to linear-stability studies, there is a critical value f^* at which the real part of one of the eigenvalues of the system changes sign and becomes positive. The system is unstable for overdrives below this critical value, with additional eigenmodes becoming unstable as f decreases. This is to be expected, since a decrease in the overdrive implies a lower postshock temperature and an increasing ratio of the activation energy over this temperature. That makes the reaction zone more sensitive to small changes of the hydrodynamic shock strength. The critical value of the overdrive factor for the above set of parameters is $f^* = 1.72$. It should also be noted that the value of the stiffness coefficient, K, is determined completely by the value of f and the normalized speed of sound ahead of the shock, $\sqrt{\gamma}$. In particular, K increases as the overdrive factor f decreases, i.e., the lower the postshock temperature, the slower the reaction becomes.

In the numerical simulations presented here, the spatial ZND profiles for various overdrive factors are evaluated and used as initial conditions. The truncation error is left to trigger the instabilities, and the evolution process is observed. The state at the left boundary is always given by the state at the end of the reaction zone at $t = 0$, that is, the left endpoint of the ZND profile. All computations are performed with $CFL = 0.5$.

As a first test, the overdrive factor is taken to be $f = 1.8$. This is a case of a stable detonation. The shock speed and stiffness coefficient for that overdrive are $D = 9.1357$ and $K = 145.69$, respectively. The time history of the shock pressure, i.e., the pressure immediately behind the shock, is presented in Fig. 10; the fluctuation of the shock pressure decays with time. The resolution for that simulation is 15 pts/$L_{1/2}$.

The results of the time history of the shock pressure are in very good agreement with the results obtained by Bourlioux *et al.* [5], using the PPM algorithm and front-tracking, with the same resolution.

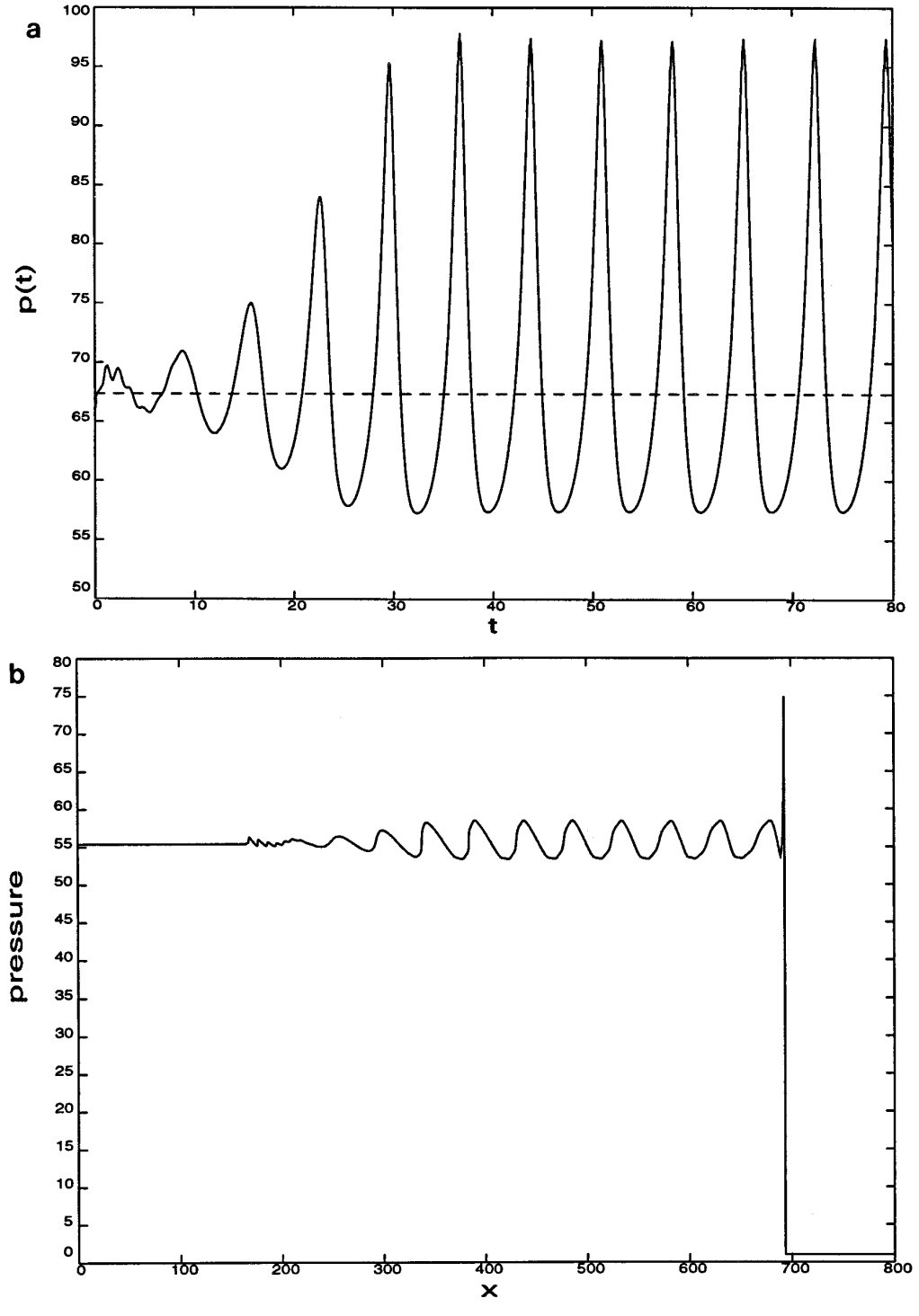

FIG. 11. (a) Shock pressure time history for a detonation with an overdrive factor, $f = 1.60$. Resolution, 20 pts/$L_{1/2}$. Horizontal line represents ZND solution. (b) Pressure spatial profile for a detonation with an overdrive factor, $f = 1.60$, at $t = 80.0$. Resolution, 20 pts/$L_{1/2}$. (c) Variation of peak pressure with grid resolution for various schemes. Detonation with overdrive factor $f = 1.60$.

Subsequently, the overdrive factor is lowered to $f = 1.6$. This case corresponds to $D = 8.6134$ and $K = 230.75$. Linear-stability analysis predicts one unstable mode for this case. The time history of the shock pressure is presented in Fig. 11a. The spatial profile of the pressure at time $t = 80.0$ is presented in Fig. 11b. Following Quirk [44], a convergence study for the peak shock pressure for various numerical schemes is performed, and the results

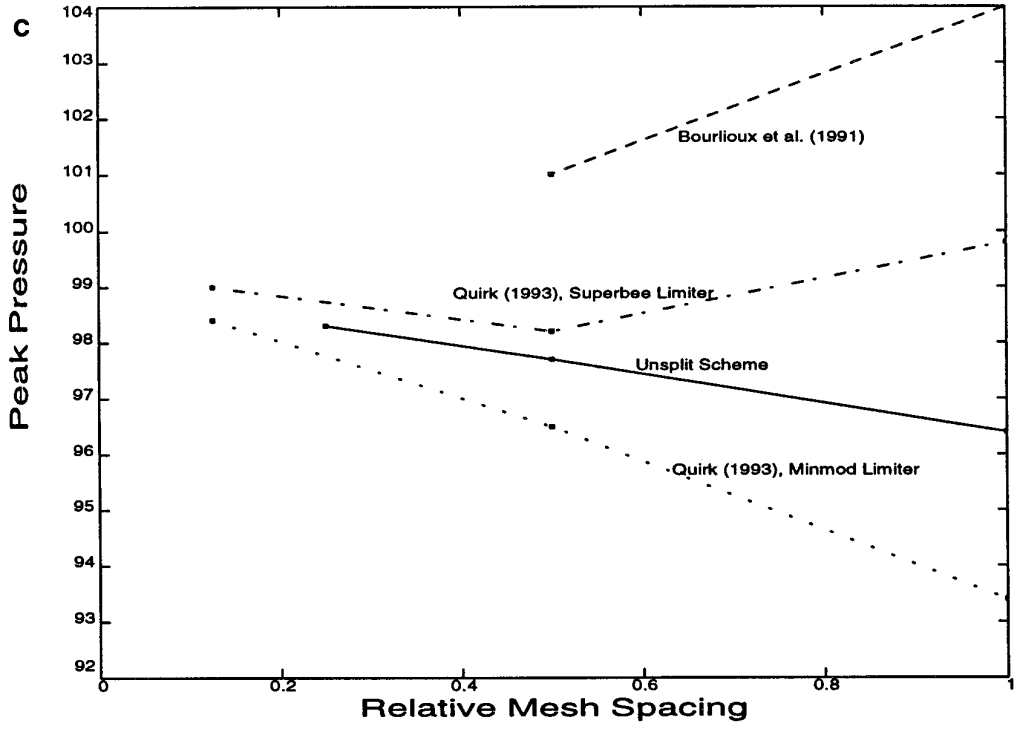

FIG. 11—*Continued*

are presented in Fig. 11c. The numerical schemes are: PPM with front-tracking and mesh refinement (Bourlioux *et al.* [5]), Roe's solver with *superbee limiter* (Quirk [44]), Roe's solver with the *minmod limiter* (Quirk [44]), and the present unsplit scheme. In this figure, a relative mesh spacing of 1 corresponds to a resolution of 10 pts/$L_{1/2}$. Similarly, a relative mesh spacing of 0.25 corresponds to a resolution of 40 pts/$L_{1/2}$. The schemes can be seen to converge to approximately the value predicted by Fickett and Wood [18], who estimated that the peak pressure is 98.6.

Subsequently, numerical results are obtained for lower overdrive factors, $f = 1.40$ and $f = 1.34$. For $f = 1.40$, the parameters are $D = 8.06$, and $K = 411.98$. Linear-stability analysis predicts two unstable modes for this case. The shock pressure history, which exhibits a period-doubling oscillation, is presented in Fig. 12a, and the spatial profile of pressure, at time $t = 100$, is presented in Fig. 12b. For $f = 1.34$, the parameters of the problem are $D = 7.88$ and $K = 504.91$. This is a case with three unstable modes, according to linear-stability analysis. The shock pressure history and the spatial profile of the pressure at $t = 100$ are presented in Figs. 13. The results for both overdrive factors are obtained with a resolution of 40 pts/$L_{1/2}$. Numerical simulations with higher resolution produce the same results in both cases.

The overdrive factor is lowered further, to a value of $f = 1.30$. The shock speed and stiffness coefficient for this detonation are $D = 7.764$ and $K = 583.71$. Linear-stability analysis suggests three unstable modes for this case. Bourlioux *et al.* [5] proposed the existence of chaotic-pulsation instabilities because they observed a sensitive dependence of the results on the initial data, as is characteristic of chaotic systems with a small number (greater-than or equal-to, 3) of degrees of freedom (e.g., Nicolis [39]). Specifically, they observed that slightly perturbed initial data produced results that are qualitatively similar but quantitatively different.

Similar behavior is demonstrated in the present study in simulations performed using the unsplit scheme. This can be verified by comparing the shock pressure history of unperturbed initial profiles, as presented in Fig. 14a, with the pressure history of perturbed initial profiles in Fig. 14b. To perform these simulations, a perturbation is added to the ZND profiles of the fluid-dynamic variables given by a sinusoidal wave of amplitude 0.1% of the values behind the shock, with unity wavelength.

Numerical simulations using high-order algorithms for even lower overdrive factors had not been published until recently. Linear stability predicts an increased number of unstable modes as f decreases. He and Lee [22] presented results obtained by a split algorithm, for overdrive factors as low as $f = 1.10$. For this case, which corresponds to a shock speed of $D = 7.1418$ and a stiffness coefficient $K =$

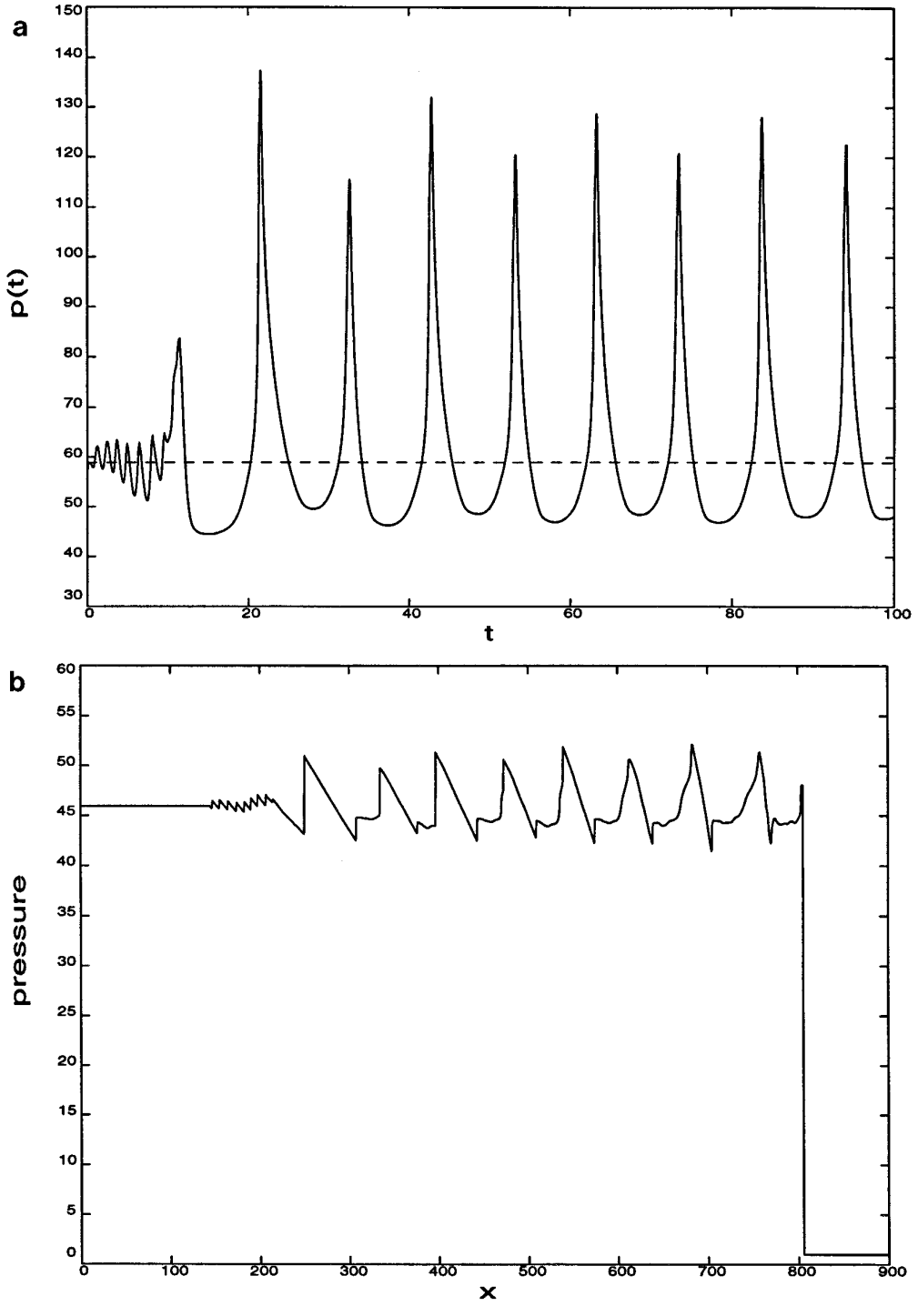

FIG. 12. (a) Shock pressure history for a detonation with an overdrive factor, $f = 1.40$. Resolution, 20 pts/$L_{1/2}$. Horizontal line represents ZND solution. (b) Pressure spatial profile for a detonation with an overdrive factor, $f = 1.40$, at $t = 100.0$. Resolution, 20 pts/$L_{1/2}$.

1389.58, they found that the initial perturbations die out, that the postshock values of the variables become steady, and that the reaction front lags behind the hydrodynamic shock at an ever-increasing distance (quenched detonation). They attempted a connection between the detonation quenching they observed and linear-stability analysis, noting that, at $f = 1.165$, the imaginary part of the first eigenvalue becomes zero. We note, however, that linear-

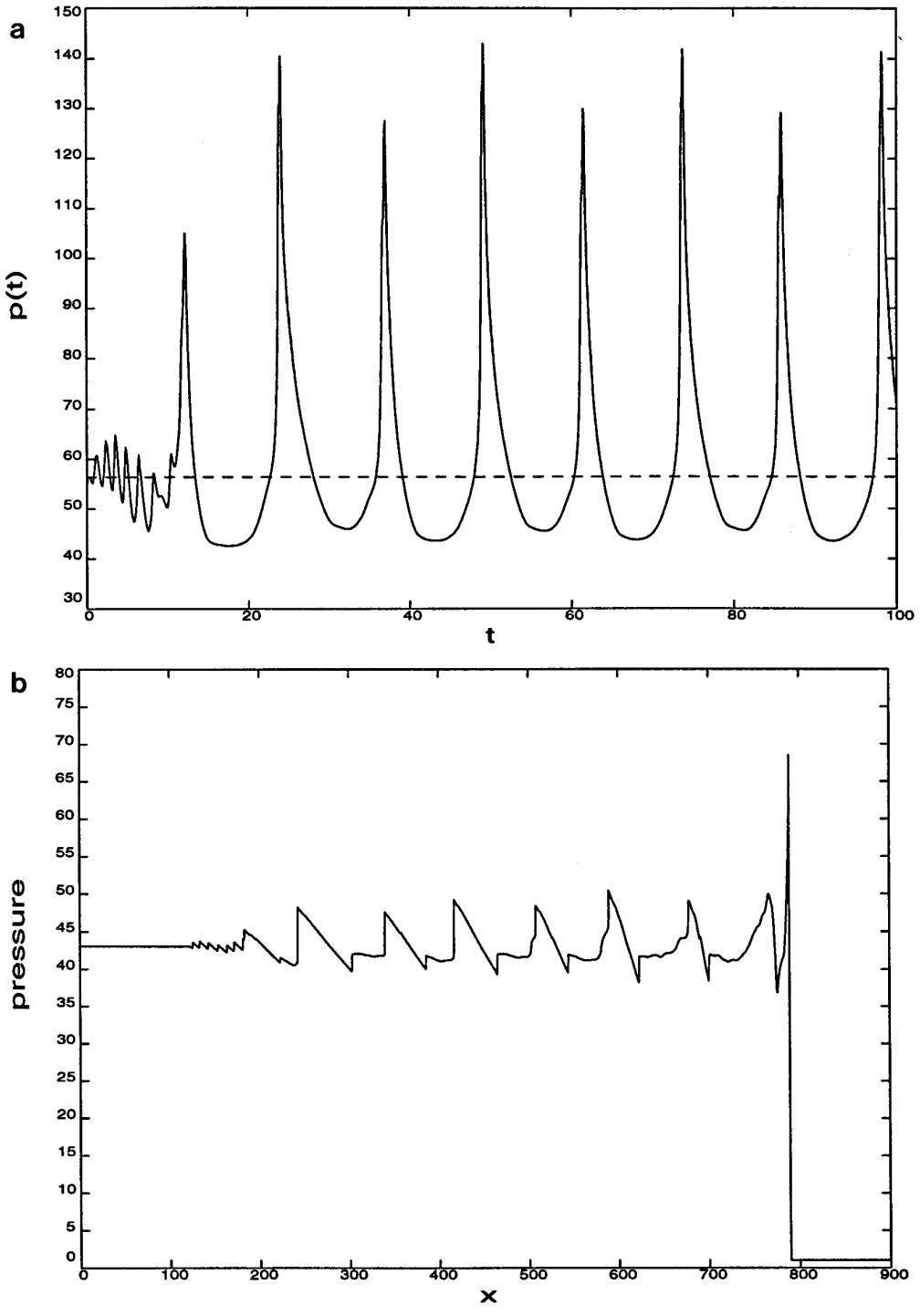

FIG. 13. (a) Shock pressure time history for a detonation with an overdrive factor, $f = 1.34$. Resolution, 20 pts/$L_{1/2}$. Horizontal line represents ZND solution. (b) Pressure spatial profile for a detonation with an overdrive factor, $f = 1.34$, at $t = 100.0$. Resolution, 20 pts/$L_{1/2}$.

stability analysis is helpful for overdrives close to f^* and not for overdrives close to unity.

Furthermore, this system of equations cannot produce a quenched detonation at large times. This is because of the phenomenon of thermal runaway; the reaction front stays temporarily behind the main shock and the temperature in the area between the reaction front and the shock is low. In this area, therefore, the source term on the right-

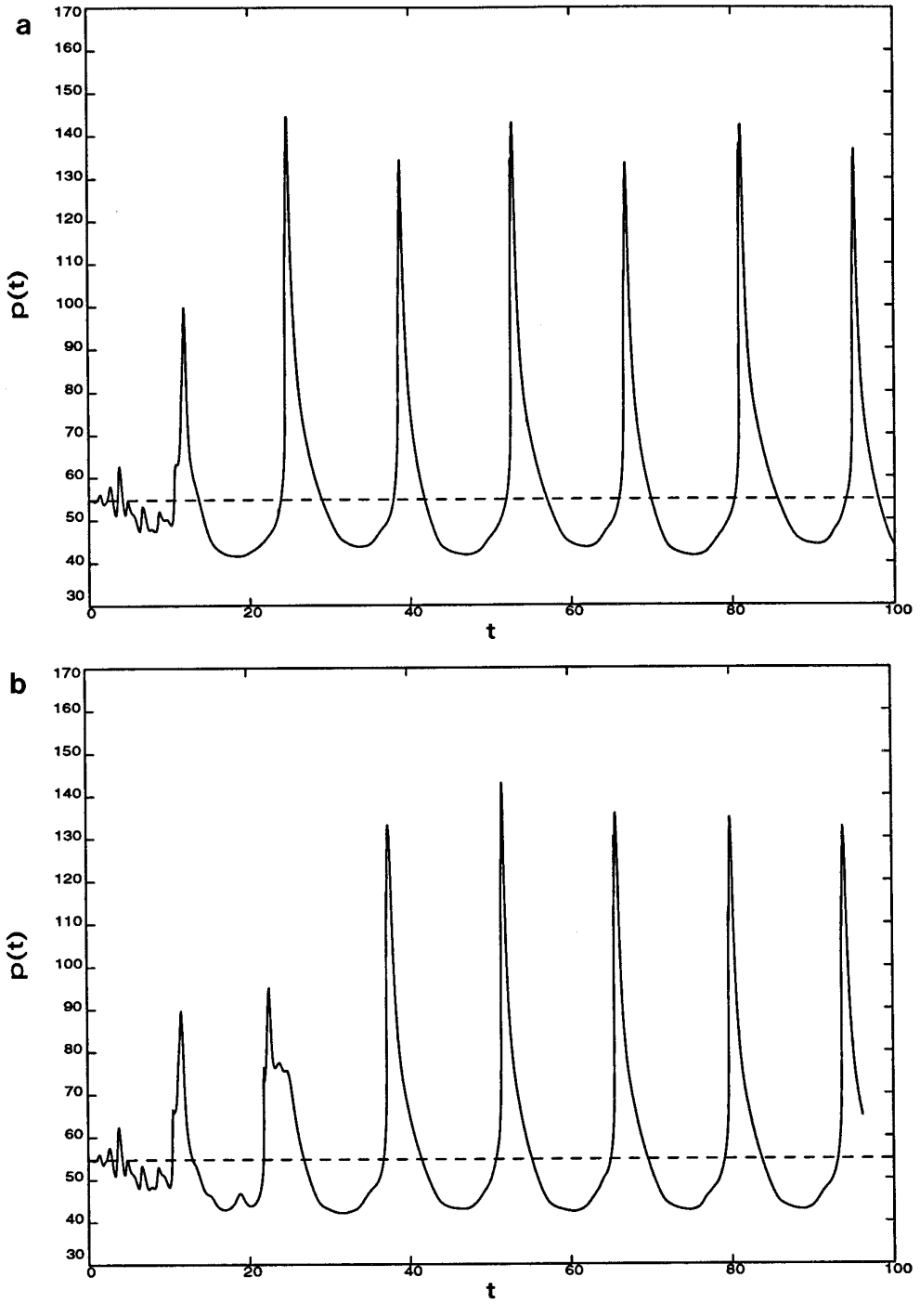

FIG. 14. (a) Shock pressure time history for a detonation with an overdrive factor, $f = 1.30$. Resolution, 80 pts/$L_{1/2}$. Horizontal line represents ZND solution. (b) Shock pressure time history for a detonation with an overdrive factor, $f = 1.30$, and perturbed initial data. Resolution, 80 pts/$L_{1/2}$. Horizontal line represents ZND solution.

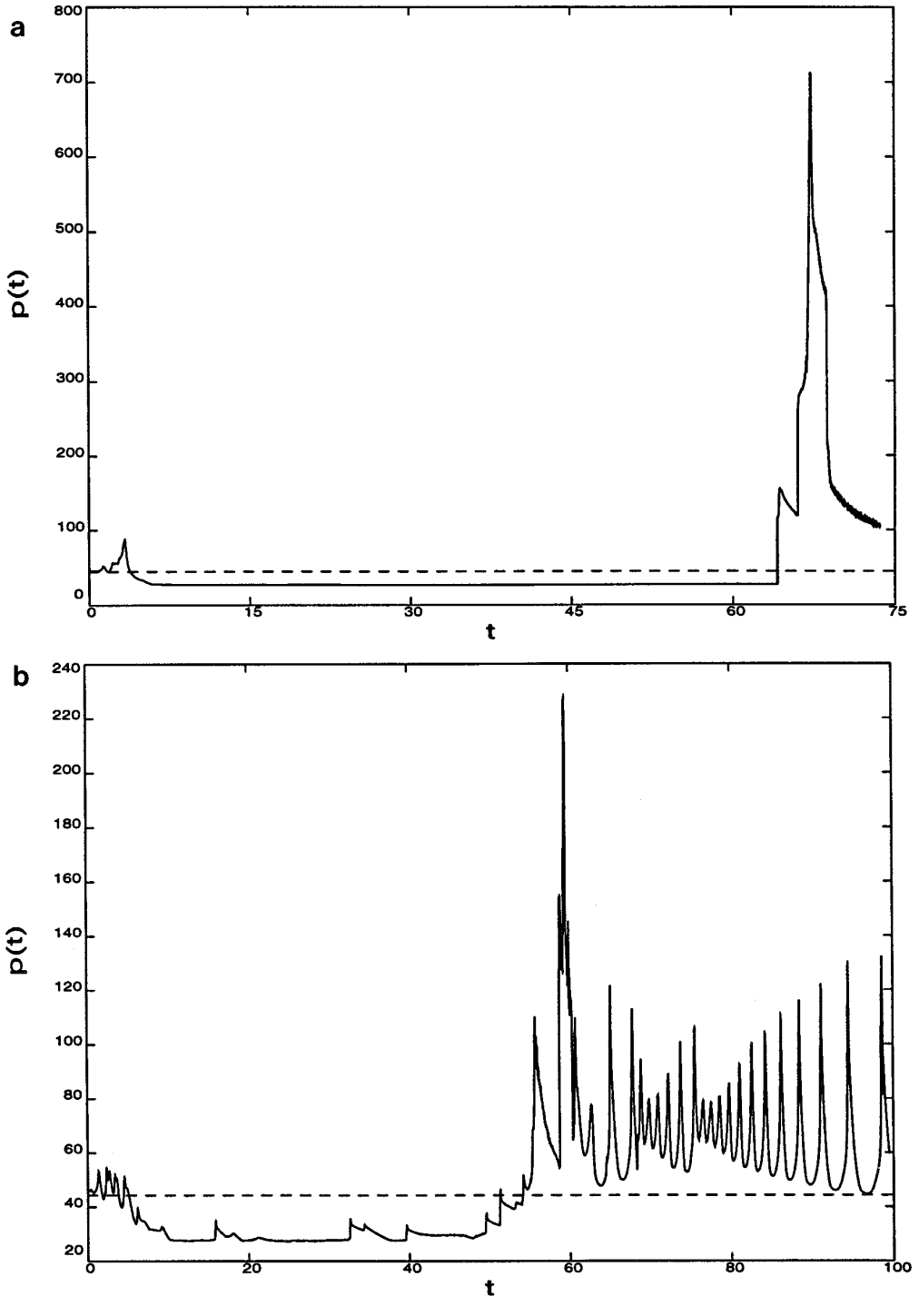

FIG. 15. (a) Shock pressure time history for a detonation with an overdrive factor, $f = 1.10$. Resolution, 15 pts/$L_{1/2}$. Horizontal line represents ZND solution. (b) Shock pressure time history for a detonation with an overdrive factor, $f = 1.10$. Resolution, 50 pts/$L_{1/2}$. Horizontal line represents ZND solution.

hand side of the species equation is exponentially small. The process in that region can be described as homogeneous combustion; i.e., after some time, the source term becomes large and a rapid explosion takes place, resulting in high combustion spikes.

An *underresolved* simulation for $f = 1.10$ is presented in Fig. 15a. The proposed unsplit scheme is used, with a resolution of 15 pts/$L_{1/2}$. The result is in excellent agreement with the result of He and Lee [22], obtained with a mesh of 50 pts/$L_{1/2}$, up to time $t = 60.0$ (it is at that time that He and Lee [22] stopped their simulation). The high rise of the shock pressure that occurs at time $t \simeq 65.0$ is due to the phenomenon of thermal runaway discussed above.

When the resolution is increased in the current simulations, a dramatic change takes place (see Fig. 15b). The temporal profile of the shock pressure becomes irregular, with no evident structure. At time $t \simeq 8.0$, the shock pressure drops to a value around $p \simeq 27.0$. The temperature at this point is around $T \simeq 3.4$, which is indeed too low to initiate and sustain the chemical reaction. Consequently, the reaction front is convected by the flow and stays behind the hydrodynamic shock.

In the region between the reaction front and the shock, however, the temperature is not constant. It can be verified that there are small pockets of material with higher temperatures (see Fig. 16a). Recall that the initial fluctuations in the shock pressure produced shock waves that travelled upstream (these waves can be seen in Fig. 16). These waves interacted with each other and some reflected back, travelled downstream, and created the temperature gradients in the region discussed above. Higher temperature points are responsible for chemical-reaction initiation. The area between the initial reaction front and the hot spot remains inert. It develops to a pocket of unreacted material as soon as the hot spot has burnt completely.

In the beginning, the reaction inside the pocket is slow because the source term in the species equation is still exponentially small. This early stage of the combustion can be considered as a constant-pressure process. When the source term becomes larger, however, a relatively rapid explosion occurs. During this stage of combustion, the density is initially almost constant (for inertial reasons) with the temperature rise producing a large pressure rise. This pressure rise, however, produces two shock waves, one travelling downstream and one upstream. The downstream shock wave catches up with the main shock. The time required for this to take place can be estimated by the shock-pressure history; cf. Fig. 15b. In this figure, the sudden jumps in shock pressure, at time up to $t \simeq 55$, correspond to the overtakings of the main front by shocks produced during earlier explosions. The increase of the shock pressure restarts the detonation process behind the shock, until it drops again to a value $p \simeq 27.0$. The shock wave that propagates upstream causes the explosion of the pocket of unreacted material. This second explosion gives birth to a second pair of shock waves. Spatial profiles of the flow variables during such an explosion are given in Figs. 17.

This process repeats itself, until $t \simeq 55$, when the explosions become large. After that, the detonation oscillates in an irregular way and appears to correspond to the situation termed ''spatial and temporal chaos'' (e.g., Nicolis [39]). Resolutions up to 250 pts/$L_{1/2}$ are used for this case. It is observed that resolutions finer than 15 pts/$L_{1/2}$, produce qualitatively similar, but quantitatively different, results at large times. In such highly unstable cases, different resolutions are equivalent to different initial conditions. Further numerical investigations, with much higher resolutions, would be required for a definitive conclusion, even though the present numerical evidence indicates that the detonation does not quench and that the system exhibits chaotic behavior for $f = 1.10$.

4. CONCLUDING REMARKS

A new approach for evolving hyperbolic systems with source terms has been presented. Performing the decomposition of the equations to a set of scalar fields along selected paths in space-time, it is possible to identify associated invariants along these paths that permit the construction of unsplit algorithms for the numerical integration of these laws.

The proposed scheme was tested on a scalar conservation law with a nonlinear source term and on the one-dimensional compressible. Euler equations for reacting flows. The scheme is found to be accurate and robust. In the scalar case, increased stiffness may, depending on the initial data, produce continuous solutions with high propagation velocities. Unless the computational grid is sufficiently resolved, these velocities may not be captured correctly with explicit schemes. Overall, the proposed unsplit scheme is more accurate than the equivalent split version.

In the case of reacting flows, useful insight for the evolution of detonations in the unstable regime was obtained. The question of the long time behavior of detonations near the CJ point is still open. Results obtained by the present scheme indicate chaotic behavior of the system, in contrast with recent previous predictions.

An advantage of the new approach is that it can be generalized to multidimensional flows, in a straightforward way. The system of conservation laws can be decomposed to a set of homogeneous ODEs, as in the 1D case, that hold along selected manifolds in (x, y, t) space. The study of the geometry of these manifolds and the design of unsplit multidimensional algorithms, is the subject of work presently in progress.

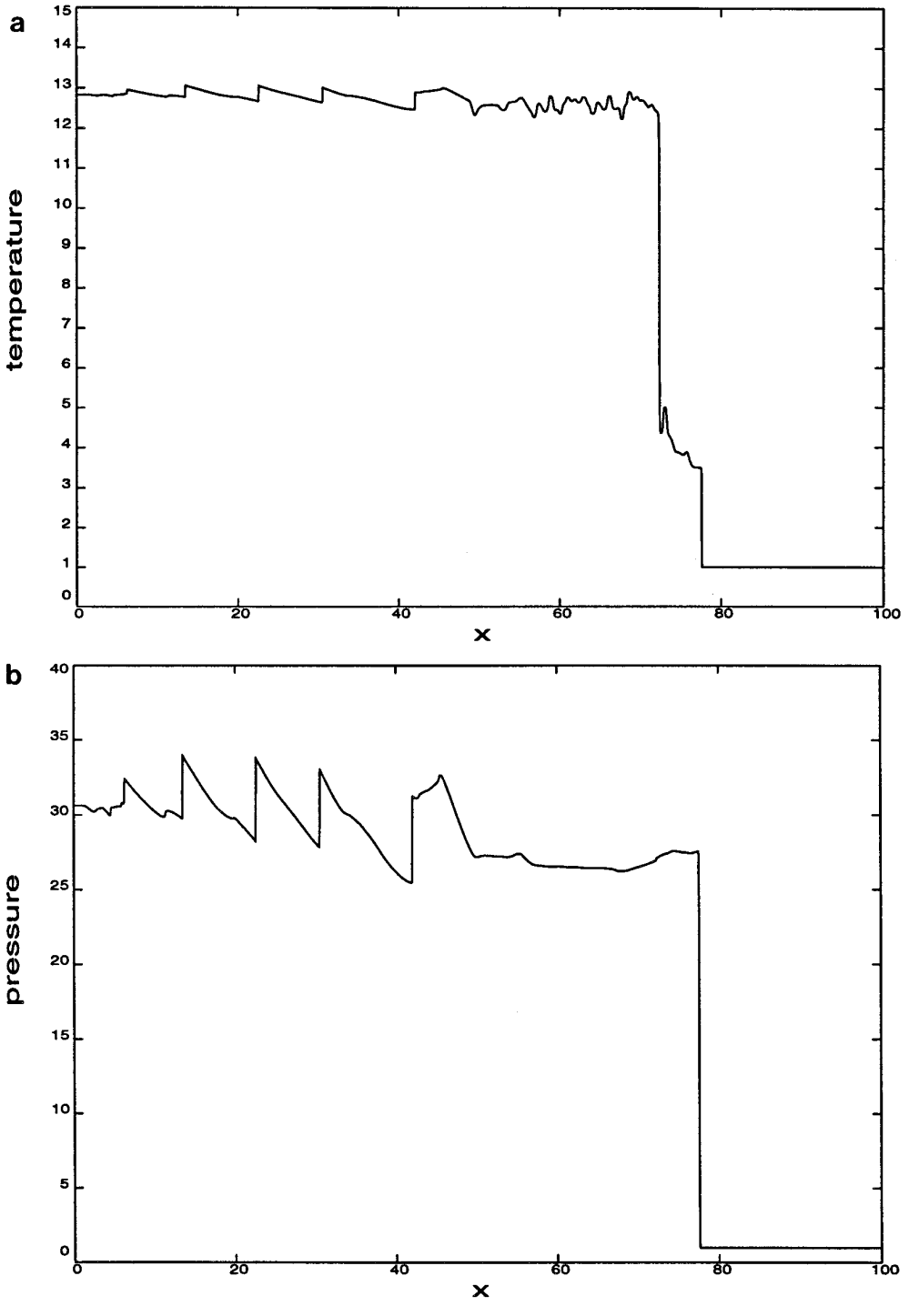

FIG. 16. (a) Temperature spatial profile for a detonation with an overdrive factor, $f = 1.10$, at $t = 12.0$. Resolution, 50 pts/$L_{1/2}$. (b) Pressure spatial profile for a detonation with an overdrive factor, $f = 1.10$, at $t = 12.0$. Resolution, 50 pts/$L_{1/2}$.

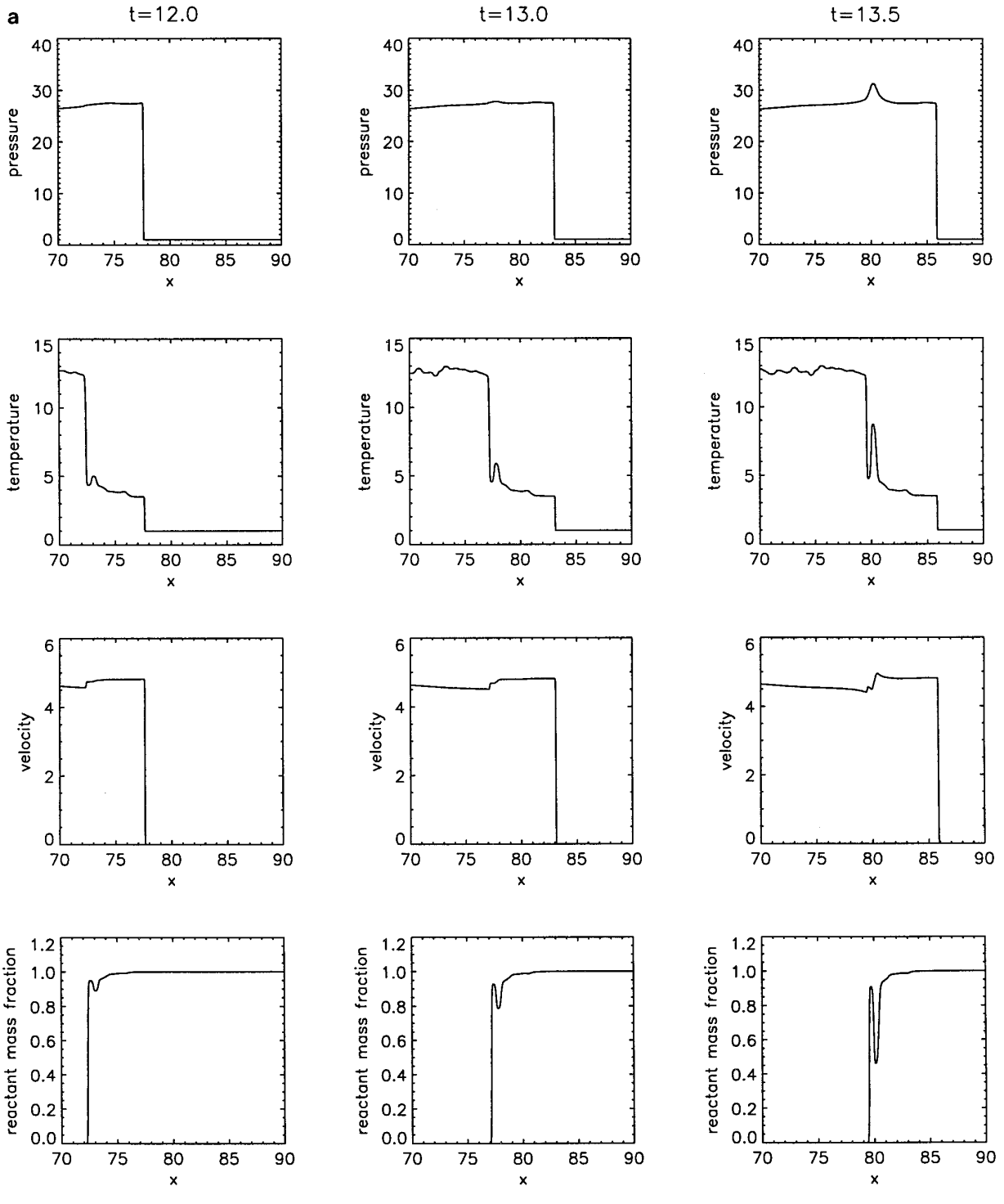

FIG. 17. Spatial profiles of the flow variables at the area of an explosion, for a detonation with overdrive factor, $f = 1.10$. (a) Profiles at $t = 12.0, 13.0, 13.5$. Resolution, 50 pts/$L_{1/2}$. (b) Profiles at $t = 14.0, 15.0, 16.0$ Resolution, 50 pts/$L_{1/2}$.

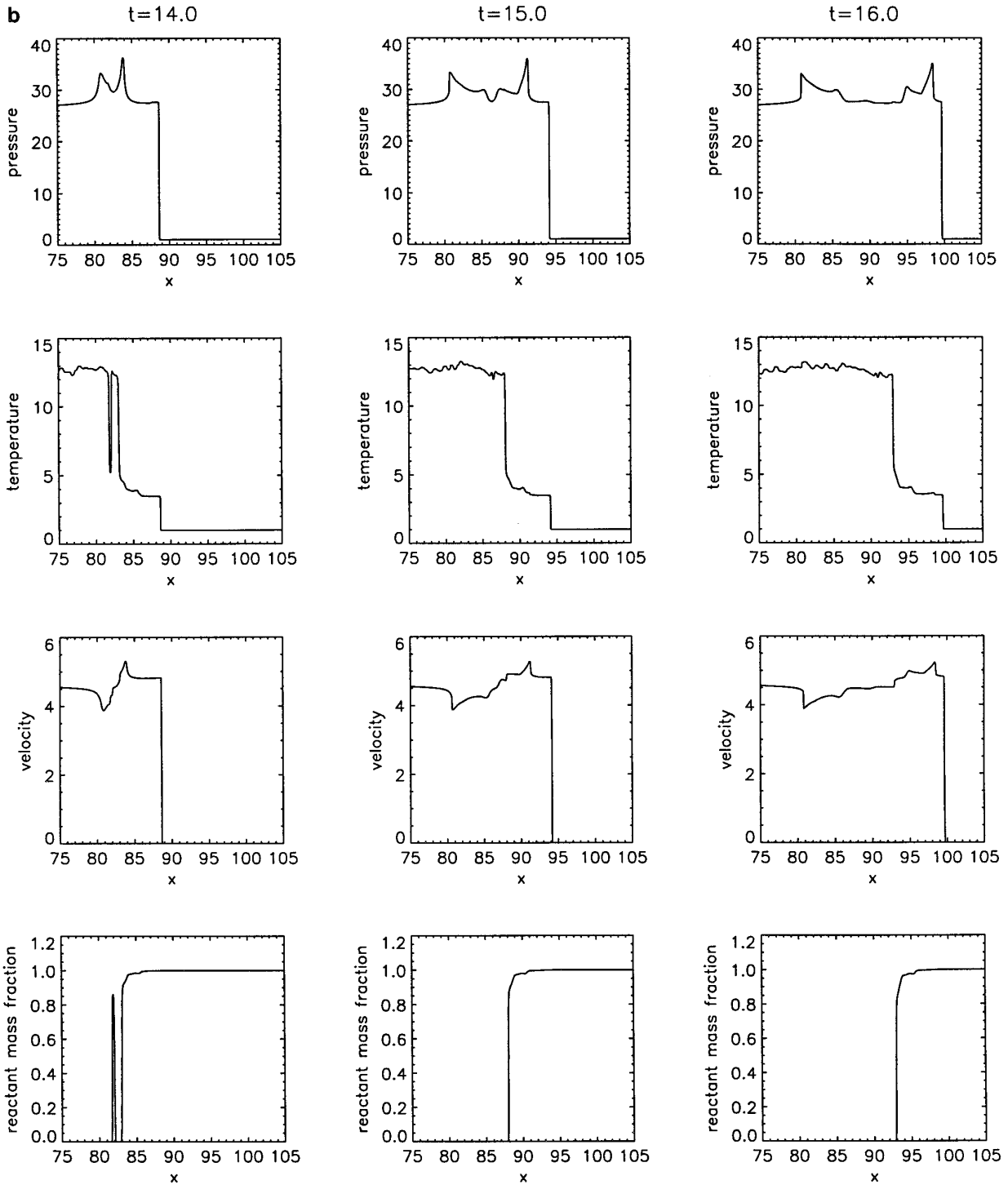

FIG. 17—*Continued*

ACKNOWLEDGMENTS

The authors thank Dr. Tasso Lappas and Professor Joseph Shepherd for many stimulating discussions and the anonymous referees of this paper for their comments and insightful suggestions. This work is part of a larger effort to understand mixing and combustion, sponsored by the Air Force Office of Scientific Research Grants F49620-94-1-0353 and F49626-93-1-00338, whose support is gratefully acknowledged.

REFERENCES

1. G. Abouseif and T. Y. Toong, Theory of unstable one-dimensional detonations, *Combust. Flame* **45,** (1982).
2. Ben-Artzi, M., The generalized Riemann problem for reactive flows, *J. Comput. Phys.* **81,** (1989).
3. M. Ben-Artzi and J. Falcovitz, An upwind second-order scheme for compressible duct flows, *SIAM J. Sci. Stat. Comp.* **7,** 744 (1986).
4. A. Bourlioux, *Numerical Study of Unstable Detonations,* Ph.D. thesis, Princeton University, 1991.
5. A. Bourlioux, A. J. Majda, and V. Roytburd, Theoretical and numerical structure for unstable one-dimensional detonations, *SIAM J. Appl. Math.* **51,** 303 (1991).
6. A. Chalabi, ''Stable upwind schemes for hyperbolic conservation laws with source terms, *IMA J. Num. Anal.* **12,** 217 (1992).
7. G. Chen, C. Levermore, and T. P. Liu, Hyperbolic conservation laws with stiff relaxation terms and entropy, *Comm. Pure Appl. Math.* **47,** 787 (1994).
8. Y. S. Choi and A. J. Majda, Amplification of small-amplitude high-frequency waves in a reactive mixture, *SIAM Rev.* **31,** 401 (1989).
9. P. Colella, A. J. Majda, and V. Roytburd, Theoretical and numerical structure of reacting shock waves, *SIAM J. Sci. Stat. Comp.* **7,** 1059 (1986).
10. P. Colella and P. R. Woodward, The PPM method for gas dynamic simulations, *J. Comp. Phys.* **54,** 174 (1984).
11. R. Courant and D. Hilbert, *Methods of Mathematical Physics, Vol. II,* (Interscience, New York, 1963).
12. M. G. Crandall, and A. J. Majda, Monotone differnce approximations for scalar conservation laws, *Math. Comp.* **34,** 1 (1980).
13. R. J. di Perna and A. J. Majda, The validity of nonlinear geometric optics for weak solutions of conservation laws, *Comm. Math. Phys.* **98,** 313 (1985).
14. W. Doering, On detonation processes in gases, *Ann. Phys.* **43,** 421 (1943).
15. B. Engquist and B. Sjogreen, *Robust Difference Approximations of Stiff Inviscid Detonation Waves,* UCLA-CAM Report 91-03, 1991.
16. J. J. Erpenbeck, Stability of idealized one-reaction detonations, *Phys. Fluids* **7,** 684 (1964).
17. W. Fickett and W. C. Davis, *Detonation* (U. C. Berkeley Press, Berkeley, 1979).
18. W. Fickett and W. W. Wood, Flow calculation for pulsating one-dimensional detonation, *Phys. Fluids* **9,** 903 (1966).
19. J. Glimm, G. Marshall, and B. Plohr, A generalized Riemann problem for quasi-one-dimensional gas flows, *Adv. Appl. Math.* **5,** 1 (1984).
20. D. F. Griffiths, A. M. Stuart, and H. C. Yee, Numerical wave propagation in an advection equation with a nonlinear source term, *SIAM J. Numer. Anal.* **29,** 1244 (1992).
21. A. Harten, B. Engquist, S. Osher, and S. Chakravarthy, Uniformly high order accurate ENO schemes, III, *J. Comp. Phys.* **71,** 231 (1987).
22. L. T. He and J. H. S. Lee, The dynamical limit of one-dimensional detonations, *Phys. Fluids* **7**(5), 1151 (1995).
23. A. K. Kapila, B. J. Matkowsky, and A. van Harten, An asymptotic theory of deflagrations and detonations. I. The steady solutions, *SIAM J. Appl. Math.* **43,** 491 (1983).
24. S. N. Kruzkov, First order quasilinear equations in several dependent variables, *Math. Sbornik* **123,** 217 (1970).
25. T. Lappas, A. Leonard, and P. E. Dimotakis, An adaptive lagrangian method for computing 1-D reacting and non-reacting flows, *J. Comp. Phys.* **104,** 361 (1993).
26. T. Lappas, A. Leonard, and P. E. Dimotakis, Riemann invariant manifolds for the multidimensional Euler equations, under review by the *SIAM J. Sci. Comp.* (1995).
27. P. Lax, *Hyperbolic Systems of Conservation Laws and the Mathematical Theory of Shock Waves,* (SIAM, Philadelphia, 1973).
28. P. Lax, Hyperbolic systems of conservation laws II, *Comm. Pure Appl. Math.* **10,** 537 (1957).
29. H. I. Lee and D. S. Stewart, Calculation of linear detonation instability: one-dimensional instability of plane detonation, *J. Fluid Mech.* **206,** 103 (1990).
30. R. J. Le Veque, *Numerical Methods for Conservation Laws* (Birkhauser, Zurich, 1992).
31. R. J. Le Veque and K. M. Shyue, One-dimensional front tracking based on high resolution wave propagation methods, *SIAM J. Sci. Comp.* **16,** 348 (1995).
32. R. J. Le Veque and H. C. Yee, A study of numerical methods for hyperbolic conservation laws with stiff source terms, *J. Comp. Phys.* **86,** 187 (1990).
33. P. L. Lions and P. E. Souganidis, Convergence of MUSCL and filtered schemes for scalar conservation laws and Hamilton-Jacobi equations, *Math. Comp.* **69,** 441 (1995).
34. T. P. Liu, Quasilinear hyerbolic systems, *Comm. Math. Phys.* **68,** 141 (1979).
35. T. P. Liu, Hyperbolic conservation laws with relaxation, *Comm. Math. Phys.* **108,** 153 (1987).
36. A. J. Majda and R. R. Rosales, Resonantly interacting weakly nonlinear hyperbolic waves. I. A single space variable, *Studies Appl. Math.* **71,** 149 (1984).
37. A. J. Majda and R. R. Rosales, Nonlinear mean field, high-frequency wave interactions in the induction zone, *SIAM J. Appl. Math.* **47,** 1017 (1987).
38. A. J. Majda and V. Roytburd, Numerical study of the mechanisms for initiation of reacting shock waves, *SIAM J. Sci. Stat. Comp.* **11,** 950 (1990).
39. G. Nicolis, *Introduction to Nonlinear Science,* Cambridge University Press (1995).
40. E. Oran and J. P. Boris, *Numerical Simulation of Reactive Flow* (Elsevier, New York, 1987).
41. S. Osher and J. A. Sethian, Fronts propagating with curvature dependant speed: algorithms based on Hamilton-Jacobi formulations, *J. Comp. Phys.* **79,** 12 (1988).
42. R. Pember, Numerical methods for hyperbolic conservation laws with stiff relaxation. I. spurious solutions, *SIAM J. Appl. Math.* **53,** 1293 (1993).
43. R. Pember, Numerical methods for hyperbolic conservation laws with stiff relaxation. II. Higher-order Godunov methods, *SIAM J. Sci. Comp.* **14,** 824 (1993).
44. J. J. Quirk, *Godunov-type schemes applied to detonation flows,* ICASE report No. 93-15 (1993).
45. P. H. Roe, Approximate Riemann solvers, parameter vectors, and difference schemes, *J. Comp. Phys.* **43,** 357 (1981).

46. P. H. Roe, Characteristic-based schemes for the Euler equations, *Ann. Rev. Fl. Mech.* **18,** 337 (1986).
47. P. H. Roe, ''Upwind Differencing Schemes for Hyperbolic Conservation Laws with Source Terms,'' *Lecture Notes in Mathematics,* Vol. 1270, edited by C. Carasso, P. Raviart, and D. Serre (Springer-Verlag, New York, 1986).
48. J. A. Sethian, Numerical algorithms for propagating interfaces: Hamilton-Jacobi equations and conservation laws, *J. Diff. Geom.* **31,** 131 (1990).
49. J. Smoller, *Shock Waves and Reaction-Diffusion Equations* (Springer-Verlag, New York, 1983).
50. J. Strang, On the construction and comparison of differnce schemes, *SIAM J. Num. Anal.* **5,** 506 (1968).
51. T. Tang and Z. H. Teng, Error bounds for fractional step methods for conservation laws with source terms, *SIAM J. Num. Anal.* **32,** 110 (1995).
52. B. van Leer, Towards the ultimate conservative difference scheme. IV. A new approach to numerical convection, *J. Comp. Phys.* **23,** 276 (1977).
53. B. van Leer, Towards the ultimate conservative difference scheme. V. A second order sequel to Godunov's method, *J. Comp. Phys.* **32,** 101 (1979).
54. B. van Leer, On the relation between the upwind-differncing schemes of Godunov, Engquist-Osher and Roe, *SIAM J. Sci. Stat. Comp.* **5,** 1 (1984).
55. J. von Neumann, Theory of detonation waves, *John Von Neumann Collected Works,* Vol. 6, Macmillan, New York (1942).
56. H. C. Yee, *A class of high-resolution explicit and implicit shock-capturing methods,* Von Karman Institue, Belgium (1987).
57. Y. B. Zeldovich, *On the Theory of the Propagation of Detonation in Gaseous Systems,* NACA TM 1261, 1960. [English translation]